Taxonomy and toxicity of a bloom-forming Ostreopsis species (Dinophyceae, Gonyaulacales) in Tahiti island (South Pacific Ocean): one step further towards resolving the identity of O. siamensis.

Nicolas Chomérat, Gwenael Bilien, Jérôme Viallon, Fabienne Hervé, Damien Réveillon, Kévin Henry, Mayalen Zubia, Christophe Vieira, André Ung, Clémence Mahana Iti Gatti, et al.

Taxonomy and toxicity of a bloom-forming *Ostreopsis* species (Dinophyceae, Gonyaulacales) in Tahiti island (South Pacific Ocean): one step further towards resolving the identity of *O. siamensis*.

Nicolas Chomérat[1*], Gwenael Bilien[1], Jérôme Viallon[2], Fabienne Hervé[3], Damien Réveillon[3], Kévin Henry[2], Mayalen Zubia[4], Christophe Vieira[5], André Ung[2], Clémence Mahana iti Gatti[2], Mélanie Roué[6], Amélie Derrien[1], Zouher Amzil[3], Hélène Taiana Darius[2], and Mireille Chinain[2]

[1]IFREMER, LER BO, Station of Marine Biology of Concarneau, Place de la Croix, F-29900 Concarneau, France

[2]Institut Louis Malardé, Laboratoire des Micro-algues toxiques, UMR 241-EIO, PO box 30, 98713 Papeete, Tahiti, French Polynesia

[3]IFREMER, Phycotoxins Laboratory, BP 21105, F-44311 Nantes Cedex 3, France

[4]Université de Polynésie Française, UMR 241-EIO, PO Box 6570, 98702 Faa'a, Tahiti, French Polynesia

[5]Kobe University Research Center for Inland Seas, Rokkodai, Kobe 657-8501, Japan

[6]Institut de Recherche pour le Développement (IRD), UMR 241-EIO, PO box 529, 98713 Papeete, Tahiti, French Polynesia

[*]Corresponding author: nicolas.chomerat@ifremer.fr

Abstract

Among dinoflagellates responsible for benthic harmful algal blooms, the genus *Ostreopsis* primarily described from tropical areas has been increasingly reported from subtropical and temperate areas worldwide. Several species of this toxigenic genus produce analogs of palytoxin, thus representing a major threat to human and environmental health. The taxonomy of several species needs to be clarified as it was based mostly on morphological descriptions leading in some cases to ambiguous interpretations and misidentifications. The present study aims at reporting a benthic bloom that occurred in April 2019 in Tahiti island, French Polynesia. A complete taxonomic investigation of the blooming *Ostreopsis* species was realized using light, epifluorescence and field emission electron microscopy and phylogenetic analyses inferred from LSU rDNA and ITS–5.8S rDNA regions. Toxicity of a natural sample and strains isolated from the bloom was assessed using both neuroblastoma cell-based assay and LC-MS/MS analyses. Morphological observations showed that cells were round to oval, large, 58.0–82.5 µm deep (dorso-ventral length) and 45.7–61.2 µm wide. The cingulum was conspicuously undulated, forming a 'V' in ventral view. Thecal plates possessed large pores in depressions, with a collar rim. Detailed observation also revealed the presence of small thecal pores invisible in LM. Phylogenetic analyses were congruent and all sequences clustered within the genotype *Ostreopsis* sp. 6, in a subclade closely related to sequences from the Gulf of Thailand and Malaysia. No toxicity was found on the field sample but all the strains isolated from the bloom were found to be cytotoxic and produced ostreocin D, a lower amount of ostreocins A and B and putatively other compounds. Phylogenetic data demonstrate the presence of this species in the Gulf of Thailand, at the type locality of *O. siamensis*, and morphological data are congruent with the original description and support this identification.

Keywords

dinoflagellate; ITS–5.8S rDNA; LSU rDNA; microscopy; morphology; ostreocin; phylogeny

1. Introduction

Tropical regions are endemically affected by outbreaks of ciguatera fish poisoning (CFP) linked to the proliferation of the toxic dinoflagellate genus *Gambierdiscus* R.Adachi & Y.Fukuyo (Berdalet et al., 2017; Chinain et al., 2020). Other benthic dinoflagellate genera, such as *Ostreopsis* Johs. Schmidt*, Prorocentrum* Ehrenberg and *Coolia* Meunier, have been shown to regularly co-occur with *Gambierdiscus* in epiphytic/benthic assemblages in tropical areas (*e.g.*, Besada et al., 1982; Chinain et al., 2016; Smith et al., 2017). The genus *Ostreopsis* was originally described from plankton samples from the Gulf of Thailand (Schmidt, 1901), but it received little attention for about 80 years. It gained a new interest when Fukuyo (1981) conducted a survey of benthic dinoflagellates potentially responsible for CFP in islands of the Pacific region. Since this date, the number of described *Ostreopsis* species has continued to increase, with frequent occurrence reports from tropical ciguateric areas (Bagnis et al., 1985; Carlson and Tindall, 1985; Ballantine et al., 1988).

Although the first report of an *Ostreopsis* bloom in the Mediterranean by F.J.R. Taylor can be dated back to 1972 (GEOHAB, 2012), since the 90s, blooms have become more frequently mentioned along the Mediterranean Sea, Atlantic, New Zealand, Japanese, Russian and Australian coasts (*e.g.*, Tognetto et al., 1995; Vila et al., 2001; Mangialajo et al., 2008; Shears and Ross, 2009; Selina and Orlova, 2010; Cohu et al., 2011; Sato et al., 2011; Parsons et al., 2012; David et al., 2013; Accoroni and Totti, 2016; Verma et al., 2020). The apparent expansion of *Ostreopsis* for the past 30 years is mainly attributable to the species *O.* cf. *ovata* and *O.* cf. *siamensis* in temperate (Accoroni and Totti, 2016) and subtropical areas (Nascimento et al., 2012; Tibiriçá et al., 2019; Verma et al., 2020). *Ostreopsis* blooms have been consistently described as forming an apparent

brownish mucilaginous and filamentous matrix covering macroalgae or substratum, sometimes extending over large areas, and which can detach and float freely (Vila et al., 2001; Shears and Ross, 2009; GEOHAB, 2012; Tibiriçá et al., 2019).

The massive blooms of the genus *Ostreopsis* cause threats to human health in certain urbanized, temperate areas and are responsible for health concerns and beach closures (Tester et al., 2020). Respiratory illness and skin irritation have been associated with *Ostreopsis* blooms in the Mediterranean and its adjacent seas (*e.g.*, Tichadou et al., 2010; GEOHAB, 2012; Berdalet et al., 2017). These effects have been attributed to analogues of palytoxin (PlTX), a highly toxic and water soluble molecule originally described from the zoanthid *Palythoa toxica* (Moore and Scheuer, 1971). A considerable number of analogs have been identified in *Ostreopsis* spp., such as ostreocins (OSTs) (Usami et al., 1995; Terajima et al., 2018a) and ovatoxins (OvTxs) (Ciminiello et al., 2008; Tartaglione et al., 2017). However, the effects of these molecules on human health still need to be investigated more deeply (Tester et al., 2020). Indeed, OvTXs were detected in aerosols (Ciminiello et al., 2014) and can also be bio-accumulated in marine organisms (Amzil et al., 2012; Brissard et al., 2014). In tropical areas, fatalities have been attributed to PlTX-like molecules, and it has been suggested that *Ostreopsis* spp. are involved in a particular type of poisoning called clupeotoxism (Alcala et al., 1988; Onuma et al., 1999) which is still controversial (Randall, 2005). Besides effects to humans, blooms have caused mortality among benthic invertebrates such as sea urchins in Brazil (Ferreira, 2006) and New Zealand (Shears and Ross, 2009). Moreover, a negative impact of *Ostreopsis* spp. has been shown on several benthic organisms (Guidi-Guilvard et al., 2012; Neves et al., 2018; Pavaux et al., 2019), which may lead to modifications of benthic communities in the concerned areas.

Toxicity of *Ostreopsis* species has been shown to vary within and among species, from non toxic to producing up to 468 pg [total OvTXs] per cell (*e.g.*, Nascimento et al., 2012; Tartaglione et al., 2017). In addition to natural variability, some contradictory reports of their toxicity and toxin

content are likely due to the existence of cryptic species or possible misidentifications (Tester et al., 2020). Studies aiming at collecting physiological and toxicological data from genetically identified isolates of *Ostreopsis* species are critically needed (Tester et al., 2020). As emphasized by many authors (Rhodes, 2011; Parsons et al., 2012; Hoppenrath et al., 2014; Tester et al., 2020), the taxonomy of *Ostreopsis* genus is problematic and requires a major revision. One of the challenges is to reconcile traditional taxonomy based on morphological features and molecular taxonomy that has allowed to unveil several genotypes not yet fully characterized (Sato et al., 2011; Chomérat et al., 2019). Hence, resolving the issues of *Ostreopsis* taxonomy is fundamental for efficient monitoring of their distribution trends and to interpret environmental influences on their population dynamics in a context of climate change (Berdalet et al., 2017; Tester et al., 2020).

The diversity of *Ostreopsis* has been only poorly studied in the islands from the mid-Pacific, including French Polynesia since it was not considered problematic contrary to *Gambierdiscus*. To date, only two species have been reported, namely *O. ovata* Y.Fukuyo and *O. lenticularis* Y.Fukuyo (Fukuyo, 1981). Bagnis et al. (1985) investigated the population dynamics of three benthic dinoflagellates in French Polynesia and suggested that *O. lenticularis* became the major component of the reef dinoflagellate community following *Gambierdiscus* bloom. Moreover, in contrast with *Gambierdiscus*, *O. lenticularis* was suspected not to be toxic (Bagnis et al., 1985), which has been fully confirmed recently (Chomérat et al., 2019). Except for the first observations by Fukuyo (1981) in French Polynesia and New Caledonia, no additional data concerning *O. ovata* have been reported from French Polynesia and this species definitely deserves more thorough investigations. More recently, Rhodes et al. (2017) identified another genotype, *Ostreopsis* sp. 3, in the poorly studied Kermadec Islands (a New Zealand territory), 1000 km northeast of New Zealand, but genetic data also showed its presence in the Cook Islands which are closer to French Polynesia. By contrast, in the western Pacific, Sato et al. (2011) made a remarkable study and identified a wider diversity, including several undescribed genotypes that still need to be assigned taxonomically.

In April 2019, a very unusual benthic bloom was detected during a field survey conducted on the western coast of Tahiti Island. Preliminary observations revealed it was dominated almost exclusively by *Ostreopsis* cells, although some pennate diatoms were also visible. The present study provides a taxonomic identification of the *Ostreopsis* species responsible for the bloom and describes its toxic potential. To this end, scanning electron microscopy (SEM) observations combined with phylogenetic analyses were performed on field samples. In addition, the toxic status of the wild bloom sample and monoclonal cultures further established from this bloom was assessed using the mouse neuroblastoma cell-based assay (CBA-N2a) in parallel with liquid chromatography coupled with tandem mass spectrometry (LC-MS/MS) to identify the toxic compounds, if any.

2. Material and methods

2.1 Sampling area and description of the wild bloom

The benthic bloom described in this study occurred at Toaroto Beach (17.64046°S; 149.610259°W) in the municipality of Punaauia, Tahiti Island (Fig. 1). It was discovered on April 2019, at the end of the rainy season, on the reef located *ca.* 20 m off the Toaroto Beach. It covered the entire reef over a radial of *ca.* 30 m between the shore and the barrier reef, and presented as a thin, filamentous and mucilaginous brownish mat covering abiotic (*e.g.*, bedrock) and biotic substrates including macroalgae (*e.g.*, *Turbinaria ornata*, *Dictyota bartayresiana*), sponges and corals (*e.g.*, *Porites*, *Pocillopora*) (Fig. 2A–C).

The bloom was sampled between 0-2 m depth using two classical methods: cells found floating on the surface attached to mucus threads were skimmed using a dip net (100 µm porosity) positioned facing the current. Epiphytic cells of *Ostreopsis* were dislodged and collected from *T. ornata* by gently shaking macroalgal samples nearby a dip net. The sea water temperature at the time of sampling was 27 °C. Both samples were then pooled and transferred into a 1 L double-cap

147 container. Three sub-samples were taken for further *in vitro* culturing assays, SEM observations
148 (preserved in 2.5% glutaraldehyde) and DNA amplification and sequencing (preserved in Lugol's
149 solution), respectively. The remaining bloom sample was freeze-dried for 20 h at -20°C, 1 mbar,
150 then 4 h at -60°C, 0.01 mbar (Martin Christ, Beta 1-8 LDplus). The resulting dry sample was
151 weighted (11 g) and stored at 4°C until further extraction.

152

153 *2.2 In vitro culturing of* Ostreopsis

154 *Ostreopsis* clonal cultures were established from single cells isolated from field samples of the
155 bloom, using an inverted microscope. They were routinely maintained in Fernbach flasks seeded
156 with 100 mL of cell inoculum and 1 L of f10k enriched natural seawater (NSW) culture medium
157 (Holmes et al., 1991), at 26 $\pm$ 1 °C, a salinity of 36, under 60 $\pm$ 10 µmol photons $m^{-2}s^{-1}$ irradiance,
158 in a 12 h light:12 h dark photoperiod. After a growth period of ≈ 35 days, cells were harvested at
159 their stationary growth phase by filtration and centrifugation. Cell counts were achieved using a
160 Coulter counter (Beckman) and the resulting cell pellets freeze-dried and weighted for toxicity and
161 toxin analyses.

162 Eight strains were analyzed in the present study (PNA19-1 to -4 and PNA19-6 to -9). These
163 strains are part of the algal collection of the Laboratory of Marine Biotoxins of the Institut Louis
164 Malardé (Tahiti, French Polynesia), where cultures are deposited. All the following experiments
165 were conducted on non-axenic acclimated batch cultures.

166

167 *2.3 Microscopy observations*

168 Light microscopy (LM) observations were conducted on live cells of 5-10 days of age using a
169 Leica DMLB microscope (Leica, Wetzlar, Germany) equipped with a D850 DSLR camera (Nikon,
170 Tokyo, Japan). Epifluorescence images were realized with a Universal microscope (Zeiss,

Oberkochen, Germany) after staining cells with Solophenyl Flavine 7GFE500. A small drop of the stock solution (0.1% w/v) was added to a drop of water containing isolated cells fixed in Lugol's solution. Epifluorescence observations were carried out using a FITC (blue excitation/green emission) filter set (Chomérat et al., 2017).

Cells isolated from the bloom were observed using field-emission SEM (FE-SEM). Prior to scanning electron microscopy, cells fixed in 2.5% glutaraldehyde from the field sample were first isolated using a micropipette, rinsed several times in distilled water and processed according to Chomérat and Couté (2008). Briefly, cells were trapped between two polycarbonate membranes (Isopore RTTP, pores 1.2 µm, Merck Millipore, Molsheim, France) attached with a paper clamp, so they can be processed with minimum losses. Dehydration was carried out in ethanol baths of 15%, 30%, 50%, 70%, 95% vol. ethanol (about 20 min in each bath), and several baths of absolute ethanol (100%) and then cells were critical point dried using an EMS 850 (Electron Microscopy Sciences, Hatfield, PA, USA) critical point drier. Dried membranes were then mounted onto 12 mm SEM stubs using carbon adhesive and coated with gold using a Cressington 108Auto (Cressington, Watford, UK) sputter coater. Cells were then observed using a FE-SEM Zeiss SIGMA 300 (Carl Zeiss Microscopy GmbH, Jena, Germany). Measurements were realized directly with the microscope or on digital images using ImageJ software (Rasband, 1997). For measurements of the curved apical pore plate (Po), the arc length was measured in apical view.

2.4 DNA amplification and sequencing

For DNA amplification, direct cell PCR approach was applied using single cells from bloom sample fixed in Lugol's solution, or a few cells from the cultures in early exponential growth phase preserved in ethanol 70%. Under the inverted microscope, fixed cells were pipetted and rinsed in several drops of nuclease-free distilled water, and then transferred into a 0.2 mL PCR tube.

Due to the low amount of DNA, a first round of PCR was realized using ITS-FW (Nézan et al., 2014) and Dino-RB (5′-TTGGGACTTCTGCGTCTCAA-3′, this study) primers , allowing the amplification of the ITS1–5.8S rDNA region (ITS1–5.8S–ITS2), LSU rDNA D1–D3 and D8–D10 regions. A second round of PCR (nested PCR) was realized using 1 µl of the amplicon produced in the first step as template. Primers used for the second amplification are given in Nézan et al. (2014) and Chomérat et al. (2019). PCR reactions were realized in 20 µL using KOD Hot Start Master Mix (Novagen-Merck KgaA, Darmstadt, Germany), according to the manufacturer's instructions. For both PCR rounds, the cycling conditions comprised an initial 2 min heating step at 95°C to activate the polymerase, followed by 30 cycles of 95 °C for 20 sec, 50 or 56 °C depending on primers, for 20 s, and a final extension at 70 °C for 150 sec. For Prior to sequencing, amplicons were visualized on an agarose gel after electrophoresis and the positive samples were purified using the ExoSAP-IT PCR Product Cleanup reagent (Affymetrix, Cleveland, OH, USA).

For sequencing of the amplicon generated at the second PCR round, the Big Dye Terminator v3.1 Cycle Sequencing Kit (Applied Biosystems, Tokyo, Japan) was used after removal of the primers and excess dye-labeled nucleotides using the Big Dye X-terminator purification kit (Applied Biosystems, Foster City, CA, USA). Sequencing products were run on an ABI PRISM 3130 Genetic Analyzer (Applied Biosystems). Forward and reverse reads were obtained.

2.5 Alignment and phylogenetic analyses

For the three genetic markers studied, parameters of the matrices used for phylogenetic analyses are given in Supplementary Table S1. Alignments were realized using the MAFFT algorithm with the selection of the q-ins-i strategy (Katoh and Standley, 2013).

Prior to phylogenetic analyses, the search for the most appropriate model of sequence evolution has been performed using jModeltest2 v. 2.1.7 (Darriba et al., 2012). Two methods of phylogenetic

reconstruction were used. Maximum Likelihood analysis (ML) was performed using PHY-ML v. 3 software (Guindon et al., 2010), and a bootstrap analysis (1000 pseudoreplicates) was used to assess the relative robustness of branches of the ML tree. Bayesian Inference analysis (BI) was realized using MrBayes 3.1.2 software (Ronquist and Huelsenbeck, 2003). Parameters of the models for ML and BI analyses are given in Supplementary Table S1.

Genetic distance (uncorrected genetic *p* distance) calculations among and within the *Ostreopsis* clades were estimated from the LSU rDNA D8–D10, LSU rDNA D1–D3 and ITS–5.8S rDNA matrices used for phylogenetic analyses, using the *p*-distance model in MEGA X: Molecular Evolutionary Genetic Analysis across Computing Platforms v. 10.0.5 (Kumar et al., 2018). Gaps and missing data were treated with the pairwise deletion option in MEGA X.

2.6 Toxicity analysis

2.6.1 Extraction procedures

The field sample (bloom) and eight clonal strains of *Ostreopsis* were further tested for their toxicity. Aliquots of 15 mg of freeze-dried cultured cell pellets corresponding to a total cell biomass $\approx 10^6$ cells, and 50 mg of the freeze-dried field sample were extracted under sonication in 670 µL of methanol (MeOH)/water (1:1, v/v) for 15 min in an ice bath. Once cell disruption was completed, the sample was centrifuged at 10,000 g at 4 °C for 10 min. The resulting supernatant was carefully recovered and the cell pellet extracted again in 670 µl of MeOH/water (1:1, v/v). Both supernatants were pooled (total volume recovered: ≈2 mL) and centrifuged at 10,000 g at 4 °C for 15 min. Finally, a 1.6 mL aliquot was sampled, evaporated to dryness at room temperature under nitrogen flux, and weighed. Supplementary Table S2 gives dry extract weight (DEW) obtained for each dry extract following this extraction step. Each dry extract was resuspended in MeOH/water (1:1, v/v) at a concentration of 10 $mg \cdot mL^{-1}$ and stored at -20°C until tested for further toxicity analyses.

243

244 *2.6.2 Neuroblastoma cell-based assay (CBA-N2a)*

245 The toxicity of *Ostreopsis* samples was assessed using the CBA-N2a following the protocol
246 previously described in Chomérat et al (2019). First, a qualitative screening was performed by
247 testing each extract at a unique concentration of 47,619 ng·mL^{-1} (corresponding to 10 µL of a 1:10
248 dilution of each dry extract stock solutions) in the absence vs. presence of 200 µM ouabain (final
249 concentrations) (O^- and O^+ conditions, respectively), each point run in triplicate in a single
250 experiment. Next, quantitative CBA-N2a analyses were conducted only on extracts showing a
251 cytotoxic activity. For each toxic extract, eight distinct concentrations ranging from 8.7 to 19,047.6
252 ng·mL^{-1} for cell samples and 4.4 to 9,523.8 pg·mL^{-1} for a standard of PlTX (Wako, Ref. 165-26141)
253 were tested in triplicate in three independent experiments, to obtain full dose-response curves.
254 Following a 20–22 h incubation period, cell viability was assessed using 3-(4,5-dimethylthiazol-2-
255 yl)-2,5-diphenyl tetrazolium bromide (MTT) assay according to Darius et al. (2018). Resulting
256 coloration was measured at 570 nm on a plate reader (iMark Microplate Absorbance Reader,
257 BioRad, Marnes-la-Coquette, France). One microplate in three independent experiments were
258 examined for the purpose of inter-assay variability comparison, allowing the calculation of
259 coefficient of variation (CVs).

260 For each quantitative CBA-N2a, the absorbance data for PlTX standard and cell extracts were
261 fitted to a sigmoidal dose-response curve (variable slope) based on the 4-parameter logistic model
262 (4PL), allowing the calculation of EC_{50} values defined as the concentration inducing 50% of
263 viability between the top and bottom of the curve, using Prism v8.1.2 software (GraphPad, San
264 Diego, CA, USA). The toxicity (T) of *Ostreopsis* sp. 6 samples (expressed in pg PlTX equiv. cell^{-1})
265 was estimated using the following formula: $T = (EC_{50,PlTX}/EC_{50,sample}) \times (DEW/\text{total biomass}$
266 analyzed).

267

268 *2.6.3 Liquid Chromatography coupled with tandem Mass Spectrometry (LC-MS/MS)*

269 Aliquots of the aqueous methanolic extracts from the 8 strains and 1 field sample used for the
270 CBA-N2a test were screened for the presence of PlTX and related known structural analogues at
271 Ifremer Phycotoxins Laboratory (Nantes, France). After resuspension in MeOH 50%, extracts were
272 ultrafiltered (0.20 µm, Nanosep MF, Pall, Mexico). LC-UV-MS/MS analyses using the MRM
273 (Multiple Reaction Monitoring) mode of acquisition were conducted as in Chomérat et al. (2019)
274 with minor modifications. In total, two LC-MS/MS and one LC-UV-MS/MS methods were used to
275 detect PlTX, 42-OH-PlTX, 12 OvTXs (-a to -k), 4 OSTs (OST-A, -B, -D and -E1), 3 McTXs (A to
276 C) and OTX-1 and -3.

277 A focus was performed on OSTs and the following precursors giving fragment A (*m/z* 313.2)
278 were added: *m/z* 1317.2; 1309.2; 1300.2 and 878.5; 873.1; 867.1 (corresponding to $[M+2H-H_2O]^{2+}$
279 and $[M+3H-H_2O]^{3+}$ ion species for OST-A/-B, -D and -E1, respectively).

280 To confirm the identity of OSTs, we used both the EPI (Enhanced Product Ion) mode of
281 acquisition on the $[M+2H-H_2O]^{2+}$and $[M+2H]^{2+}$ precursors (CE = 20 eV) and LC-HRMS (High
282 Resolution Mass Spectrometry) as in Georges des Aulnois et al. (2019).

283 **3. Results**

284 *3.1 Morphology of* Ostreopsis *cells*

285 Microscope observations of fresh samples revealed the bloom was dominated by *Ostreopsis*
286 cells, although assemblages of diatoms dominated by *Haslea* sp. were also visible (Fig. 2D).

287 The shape of *Ostreopsis* cells from strain PNA19-9 and wild sample varied from typical tear-
288 shaped (pointing ventrally) to almost round in apical and antapical views (Figs 3A–B, D–E, 4A–D).
289 They were biconvex, flattened and undulated, with the cingulum slightly sigmoid in lateral view

(Figs 3C, G, H, 4E–I). Cells from wild sample were 58.0–82.5 µm (mean 71.5 µm; s.d. 4.5 µm, *n* = 30) deep (dorso-ventral length, DV) and 45.7–61.2 µm (mean 51.2 µm; s.d. 3.3 µm, *n* = 25) wide (width, W). The DV/W ratio was 1.1–1.5 (mean 1.4; s.d. 0.1, *n* = 23).

The thecal plate pattern was APC 3′ 7″ 6c 4?s 5‴ 2⁗, and thecal plates were clearly visible both with light epifluorescence microscopy on strain PNA19-9 (Fig. 3D–I) and SEM on the field sample (Figs 4A–I, 5A–J). The apical pore complex (APC) consisted in a narrow, elongated and slightly curved Po plate (Figs 5A-B) bearing a slit and two rows of pores. It was located parallel to the left mid-lateral to dorsal cell margin. The Po plate was 15.6–19.5 µm (mean 17.5 µm; s.d. 1.1 µm, *n* = 14) long. Related to the DV length (depth) of the cell, the Po/DV ratio was 0.22–0.27 (mean 0.25; s.d. 0.02, *n* = 14). The first apical plate (1′) was hexagonal, elongated, located mostly on the left side of the cell (Figs 3D, 4A, C). On its dorsal part, it is slightly protruding over the APC (Figs 4A, 5A–B). The second apical plate (2′) was narrow and elongated, and located below the APC, extending dorsally the Po plate and reaching the precingular plate 4″ (Figs 3I, 4H, 5A–B). The third apical plate (3′) was pentagonal in shape, in contact with 1′, 2′, 4″, 5″ and 6″ but also had a very short contact with Po plate (Figs 4A, 5A-B). Of the precingular series, 1″ plate was the smallest while 6″ plate was the largest (Figs 3D, 4A, C). All precingular plates were four-sided except 2″ and 6″ plates that were pentagonal (Fig. 4A). The cingulum was narrow, slightly descending and undulated (Figs 3C, G, 4E–I). In the ventral view, the cingulum appeared with a V shape (Fig. 4E–F) while it was slightly sigmoid in lateral views (Figs 3G–H, 4H–I). The postcingular plate series comprised 5 plates (Figs 3E, 4B, D), 1‴ being small and more conspicuously visible ventrally and laterally (Fig. 4E–H). The remaining four postcingular plates were large (Figs 3E, 4B, D). Among postcingular plates, 1‴ was three-sided (Figs 4E, G–H, 5D), 2‴ five-sided, and 3‴, 4‴ and 5‴ four-sided (Fig 4B, D, H–I). The two antapical plates were unequal in size, 1⁗ plate being small and covering part of the sulcus, while 2⁗ plate was elongated, oriented in a slightly oblique direction in

regard with the dorsoventral axis, and with its sutures with 2‴ plate and 5‴ plate nearly parallel (Figs 3E–F, 4B, D).

The cingulum consisted of 6 distinct plates not studied in detail (Fig. 4H–I). The sulcus was studied partially and four plates only could be observed. The posterior sulcal plate (Sp) was small and roughly pentagonal, in contact with the posterior right sulcal plate (Sdp), 5‴ plate, 2⁗ plate and overlapped by l⁗ plate (Fig. 5D–G). The anterior right sulcal plate (Sda) contacted at least six plates, including last cingular plate c_6 (Fig. 5E–G). It formed a conspicuous thick list oriented obliquely to the left along its suture with the anterior left sulcal plate (Ssa), below the 'ventral opening' (Vo) (Fig. 5C–G). This round opening with a thick border was 1.2–1.8 µm in diameter, and consisted in deep indentation with a Latin upsilon letter shape within Ssa plate, closed anteriorly by the epithecal 1″ plate (Fig. 5E–G). Another plate (Sdp), seen partially as a narrow extension without any thecal pore, was present between Sp and Sda plates (Fig. 5E–G). The presence of other platelets could not be revealed due to the overlap by the 1⁗ plate (Fig. 5G).

The thecal surface was smooth and plates possessed pores of two kinds. Large pores were numerous, scattered all over thecal plates and well visible in LM (Figs 3F, 4A–I, 5A–I). They consisted in round pores 0.34–0.65 µm in diameter (mean 0.46 µm; s.d. 0.07 µm; $n = 31$), surrounded by small depressions in the plates forming like a rim on the edge of the pore (Fig. 5A–B, H, I). This feature was not visible from the inside (Fig. 5J). Small pores, 49–80 nm in diameter (mean 66 nm; s.d. 8 nm; $n = 31$) were sparsely scattered on the surface of thecal plates (Fig. 5A–B, H–I) but appeared more numerous on the internal side (Fig. 5J). A density of approximately 6.9 (5.4–7.8) and 7.4 (4.1–10.9) pores per 100 μm^2 (calculated on five specimens) was observed for large and small pores, respectively. As it is generally the case, the small pores could not be seen in LM and epifluorescence microscopy due to their small size (Fig. 3F).

338 *3.2 Molecular phylogenies*

339 For the phylogenetic analyses inferred from LSU rDNA D8-D10, D1-D3, and ITS-5.8S
340 sequences, a total of 14, 6, and 6 new sequences from Tahiti, French Polynesia, as well as reference
341 sequences retrieved from GenBank, were used (i.e. LSU rDNA D8–D10: IFR19-631/IFR20-173 to
342 -178, and PNA19-1 to -4/PNA19-6 to -9 acquired from six single cells isolated from the wild bloom
343 and eight cultured strains, respectively; LSU rDNA D1–D3 and ITS-5.8S: IFR20-173 to -175 and
344 PNA19-6, -8 and -9 acquired from three single cells isolated from the wild bloom and three cultured
345 strains, respectively). Parameters of the alignment and model chosen for the analyses are
346 summarized in Supplementary Table S1.

347 Both analyses performed with ML and BI gave the same tree topology and identical
348 relationships among *Ostreopsis* clades. Hence, only the majority-rule consensus trees of the ML
349 analyses are shown (Figs 6, 7, 8).

350

351 *3.2.1 LSU rDNA D8–D10 regions*

352 All 14 sequences acquired from Tahiti clustered within *Ostreopsis* sp. 6 which was a well-
353 supported clade (ML = 98, BI = 1.00), sister to *O. lenticularis* (Fig. 6). Sequences acquired from
354 single cells of the bloom and cultured strains were nearly identical and clustered in a new subclade
355 A of *Ostreopsis* sp. 6 (Fig. 6). This subclade of 14 sequences corresponded to a sister clade of two
356 sequences from Thailand (strains TF29OS and TF25OS, subclade B) with a moderately high
357 support (ML = 95, BI = 0.90). Two sequences from Japan (strains s0587 and s0595, subclade D)
358 branched with a strong support (ML = 96, BI = 1.00) at the base of the subclades A and B. Another
359 group of five sequences from Japan (OU8, IR33, IR49, and OU11) and Korea (17JJ0906) formed a
360 subclade E which appeared as a sister clade to the subclades A, B, and D with a moderate support
361 (ML = 96, BI = 0.66) (Fig. 6).

A low genetic divergence was observed within each subclade, with *p*-distances varying from 0.000 (subclade A) to 0.002 (subclade C, Table 1). The *p*-distances between subclades showed the subclades A (Tahiti) and B (Thailand) were the most closely related with a *p*-distance of 0.002. In contrast, the subclades D and E (Japan/Korea) appeared more divergent from other subclades A and B with *p*-distances of 0.012 to 0.013 (Table 1).

3.2.2 LSU rDNA D1–D3 regions

The 6 sequences acquired from the Punaauia bloom clustered within *Ostreopsis* sp. 6 which was a fully supported clade (ML = 100, BI = 1.00), sister to *O. lenticularis* (Fig. 7). The six sequences from Tahiti formed a well-resolved subclade A within *Ostreopsis* sp. 6 (ML = 90, BI = 0.96), and two sequences from Malaysia (OlPR01, subclade B) and Viet Nam (NT013, subclade C) appeared closely related and more basal (Fig. 7). These eight sequences formed a well-supported subclade of *Ostreopsis* sp. 6 (subclades A-C) (ML = 88, BI = 1.00), and three sequences from Japan (OA21, subclade D/E?) formed a sister clade with a maximal support (Fig. 7). In absence of other sequences for other markers allowing comparisons with subclades D and E, sequences of strain OA21 are putatively ascribed to 'D/E?'.

A low genetic divergence was observed within each subclade, with *p*-distances varying from 0.001 (subclade A) to 0.023 (subclade D/E?, Table 1). The *p*-distances between subclades showed the subclades A (Tahiti) and B (Malaysia) were the most closely related with a *p*-distance of 0.032. In contrast, the subclades C (Viet Nam) and D/E? (Japan) appeared more divergent from subclades A and B with *p*-distances of 0.046 to 0.105 (Table 1).

Of note, there is currently no reference sequence for D1-D3 LSU rDNA from the Gulf of Thailand whereas only one sequence (in same subclade B with ITS–5.8S rDNA region) ascribed to '*O. lenticularis*' (already mentioned) is presently available from Malaysia (OlPR01) (Fig. 7).

386

387 *3.2.3 ITS–5.8S rDNA phylogeny*

388 All the 6 sequences acquired from Tahiti clustered as a basal subclade A within *Ostreopsis* sp. 6
389 (Fig. 8). The most closely related sequences were in subclade B which included two sequences from
390 Thailand (TF29OS and TF25OS) and two from Malaysia (OlPR01 and VGO87, Fig. 8). Two
391 sequences from Viet Nam (NT011 and NT012) were more divergent and included in the subclade C,
392 while three sequences from Japan (s0587, IR33 and OU11) formed the subclades D and E, but
393 support was low (Fig. 8).

394 Except for the subclade E, a low genetic divergence was observed within each subclade, with
395 *p*-distances of 0.002 (subclade A), 0.004 (subclade B) and 0.008 (subclade C, Table 1). The *p*-
396 distances between subclades showed the lowest *p*-distance was observed between the subclade A
397 (Tahiti) and B (Thailand/Malaysia) with a value of 0.008. In contrast, the subclade A was more
398 divergent from the subclades D (*p*-distance 0.147) and E (*p*-distance 0.127), including sequences
399 from Iriomote and Okinawa islands, Japan (Table 1).

400

401 *3.3 Toxicity and toxin analyses*

402 *3.3.1 Toxicity analyses using the CBA N2a*

403 At the screening step, no toxicity was detected in the field sample, whereas all eight strains
404 tested were found toxic in O^- and O^+ conditions. When doing quantitative analyses, the PlTX
405 standard displayed a dose-response curve with a vertical negative slope in O^- conditions and a
406 sigmoidal dose-response curve with a negative slope in O^+ conditions, giving EC_{50} values of 1,074
407 ± 23 and 156 ± 17 $pg \cdot mL^{-1}$ (n = 3), respectively (Fig. 9A). The composite toxicity of the eight
408 strains of *Ostreopsis* sp. 6 showed a pattern similar to that of PlTX standard (Fig. 9B). The

estimated toxin contents ranged from 1.73 ± 0.31 to 2.48 ± 0.22 pg PlTX equiv. $cell^{-1}$ in O^- conditions (n = 3), and from 1.08 ± 0.09 to 1.40 ± 0.14 pg PlTX equiv. $cell^{-1}$ in O^+ conditions (n = 3) (Table 2). A good reproducibility of toxin contents was observed between experiments, with coefficients of variation (CVs) ranging from 4.2 to 17.8 % in O^- conditions and from 2.9 to 10.6% in O^+ conditions (Table 2). Comparison of the toxicity data between strains indicate slight differences, with a mean toxicity of 2.16 ± 0.25 and 1.27 ± 0.12 pg PlTX equiv. $cell^{-1}$ in O^- conditions (CV of 11.5%) and O^+ conditions (CV of 9.2%), respectively. Of note, the curves obtained in O^+ conditions showed the best agreement with the 4PL model used in Graphpad software, so only these values should be considered for further comparison with the toxicity data available in the literature.

3.3.2 Analyses by LC-MS/MS

Among the PlTX-like compounds screened for, we could detect OSTs in the eight strains cultivated but not in the field field sample (Supplementary Fig. S1). Total OSTs varied from 21 to 28 pg PlTX equiv. $cell^{-1}$ (Fig. 10). The OST profile was dominated by OST-D (>90%) followed by OST-A and -B in all strains tested.

As no OST standard is commercially available, we tried to confirm the identity of OSTs by both low and high resolution mass spectrometry. While EPI scan confidently proved the identity of OST-D (Fig. S2) when compared to fragments reported by Terajima et al. (2018a), the intensity for the other analogs was unfortunately too low. In addition, exact masses obtained by HRMS analyses unambiguously confirmed the presence of OST-A and -B (Δ ppm: -3.1 to +1.9, Fig. S3). The HRMS spectra showed a characteristic pattern, with the forms $[M+2H-H_2O]^{2+}$ and $[M+H+Na]^{2+}$ being more abundant. However, the $[M+H+Na]^{2+}$ exact mass corresponding to OST-E1 was missing, suggesting its absence in the OST profile of the strains studied here. Finally, as OST-A and -B are isomers and

433 due to the absence of a published chromatogram, their identity was defined based on their retention
434 time (OST-A eluting first).

435

436 **4. DISCUSSION**

437 *4.1 Phylogeny and taxonomy of the bloom forming species from Tahiti Island*

438 *4.1.1 Phylogenetic position*

439 Molecular data and phylogenetic analyses revealed that the species responsible for the bloom
440 belongs to the *Ostreopsis* sp. 6 clade, originally proposed by Sato et al. (2011) and subsequently
441 used by several authors (Tawong et al., 2014; Zhang et al., 2018; Chomérat et al., 2019; Lee and
442 Park, 2020). So far, this genotype has been found in various areas of southwestern Asia, including
443 the Gulf of Thailand, especially at the TF site (Tawong et al., 2014) which corresponds roughly to
444 the type locality of *O. siamensis* Johs. Schmidt, in Malaysia (subclade B), Viet Nam (subclade C),
445 and several islands of Japan (subclades D-E; Sato et al., 2011). Very recently, Lee and Park (2020)
446 reported the presence of this species (subclade E) in the subtropical area of Jeju island, South
447 Korea, which is the northernmost record to date. Hence, the present study is the first report of this
448 species from the mid-Pacific area. Genetic distances among the different subclades revealed that
449 there are some divergences between the subclades, suggesting that *Ostreopsis* sp. 6 might actually
450 represent a complex of closely related species, as is the case for the *O.* cf. *ovata* clade. Nevertheless
451 further studies will be necessary to resolve this issue.

452 Sequences from French Polynesia (subclade A) appeared more closely related to the sequences
453 from the Gulf of Thailand/Malaysia (subclade B in present analyses), than to sequences from other
454 origins (Viet Nam, Japan, Korea: subclades C, D and E). Consequently, the low genetic divergence
455 between subclades A and B can likely be interpreted at an intraspecific level. For instance, the ITS–
456 5.8S region sequences of subclades A and B diverged by 0.008 which is much lower than the

457 threshold value of 0.04 proposed by Litaker et al. (2007) to separate two given dinoflagellate
458 species. In contrast, the sequences from Viet Nam and Japan (subclades C, D, E) were more
459 variable and divergent from subclades A and B (ITS *p*-distances exceeding 0.04), which suggest
460 they likely represent different species. Nevertheless, more detailed studies including comparisons of
461 the ITS2 secondary structure of the different ribotypes would be necessary to resolve this question
462 in the future.

463

464 *4.1.2 Identity of* Ostreopsis *sp. 6*

465 In previous studies, the clade *Ostreopsis* sp. 6 was left unnamed since the morphology of the
466 strains was not studied or confusing. By way of example, the phylogeny inferred from ITS–5.8S
467 region includes two sequences from Malaysia originally ascribed to *O. labens* M.A. Faust & S.L.
468 Morton (VGO897) and *O. lenticularis* (OlPR01), respectively. Of note, this latter identification later
469 proved erroneous since strain OlPR01 clusters within *Ostreospsis* sp. 6 and not with *O. lenticularis*
470 (Chomérat et al., 2019). Moreover, these sequences were almost identical to sequences from the
471 Gulf of Thailand (TF25OS and TF29OS) which likely correspond to *O. siamensis* since they were
472 acquired from the area studied by Schmidt (1901), near Koh Wai Island. Although Tawong et al.
473 (2014) did not provide a detailed morphological SEM description of strains TF29OS and TF25OS,
474 they reported a dorsoventral (DV) length (= depth) size range of 49.9–84.3 µm for TF29OS, and
475 also highlighted a conspicuous undulated shape in lateral view (Fig. 4 in Tawong et al., 2014). This
476 feature is typical of *O. siamensis* as showed by Schmidt (1901) although this author mentioned a
477 DV length of 90 µm without any indication of the size variation range. Morphological features of
478 strain TF29OS appears in good agreement with the original description but, unfortunately, it has
479 been lost (T. Nishimura, pers. comm.), so further investigations to clarify whether it could be
480 ascribed to *O. siamensis* or not, is no longer possible. However, since genetic data clearly show that

strains from the Gulf of Thailand and those from Tahiti Island (subclades B and A, respectively) belong to the same species, the present morphological data are therefore useful to complete the previous study by Tawong et al. (2014).

The specimens from the bloom at Toaroto beach, Tahiti were in the same size range than those reported for strain TF29OS by Tawong et al. (2014). The larger DV length (depth) mean value found in the present study (71.5 µm vs. 62.4 µm in Tawong et al., 2014) can easily be interpreted by our observation of field specimens from the bloom (i.e. a natural population) while Tawong et al. (2014) values were obtained from a culture. Although the size is lower than the value from the original description by Schmidt (1901), it fits perfectly with the interpretation of *O. siamensis* by Fukuyo (1981) who gave a DV length range of 60–100 µm. The single value reported by Schmidt (1901) should be considered cautiously and is likely due to the low cell densities in the plankton samples he examined at station 2 (between Koh Kahdat and Koh Kut), and even lower densities found at stations 3 and 6 (South of Koh Chang). Moreover, cell specimens from the bloom and strains from Tahiti displayed a variable outline, from almost round to tear-shaped, consistent with the original drawings by Schmidt (1901). Several authors (*e.g.*, Accoroni and Totti, 2016) hypothesized that these drawings could well represent different taxa with different shapes but this hypothesis likely results from a misinterpretation of the shape as a distinctive feature between *O. siamensis* and *O. lenticularis*. As noted previously, Fukuyo (1981) never indicated that the outline can distinguish these species (Chomérat et al. 2019). The present data confirm that such variability exists in *Ostreopsis* sp. 6, both in a field sample and in cultured strains.

Additionally, the undulated (slightly sigmoid) cingulum observed in the specimens from Tahiti Island is in good agreement with the report by Tawong et al. (2014). This remarkable feature, resulting in a slightly concave hypotheca, fits extremely well with the original drawings (Fig. 7 in Schmidt, 1901) and with the description indicating an ‘inferior valve a little concave’ (Schmidt, 1901).

The presence of conspicuous thecal pores was confirmed on the specimens from Tahiti, where larger thecal pores had a diameter of 0.34–0.65 µm, as reported for TF29OS (Supplementary Table S2 in Tawong et al., 2014). This large size makes them perfectly visible in light microscopy, which is again consistent with the drawings by Schmidt (1901) and interpretation of *O. siamensis* by Fukuyo (1981). However, our study also showed the presence of very small thecal pores that are impossible to resolve in LM, which may explain their absence both in the original description and re-interpretation of *O. siamensis* (Schmidt, 1901; Fukuyo, 1981), but also in the study by Tawong et al. (2014).

However, our observations do show several discrepancies compared to the original description of *O. siamensis* with regard to the APC and the second apical plate 2′. In the original drawing, the APC appeared rather short compared to the DV length (depth) of the cell (Po/DV of 0.22 measured in Schmidt's Fig. 5) while slightly larger values were found in our study. In comparison, Tawong et al. (2014) indicated a Po plate length of 16 µm in their Supplementary Table S2, which is in the lower range of our observations. Using the average DV value, the Po/DV of strain TF29OS was 0.26, which is in the range found in the present study. Furthermore, the apical 2′ plate appeared to be short, and nearly of the same length as Po plate in Fig. 5 by Schmidt (1901). This seems in marked contrast with our observations which described a narrow and very elongated 2′ plate reaching the dorsal precingular plate 4″. Such a long 2′ plate was reportedly observed only in *O. heptagona* and the recently described species *O. fattorussoi* and *O. rhodesiae* (Norris et al., 1985; Accoroni et al., 2016; Verma et al., 2016a). This is no longer true since extensive observations on *O.* cf. *ovata* have revealed that several populations also display a long 2′ plate (Besada et al., 1982; Parsons et al., 2012; Tibiriçá et al., 2019). Moreover, in the largest species of the genus, *O. mascarenensis*, our previous study showed that the 2′ plate is actually long and it reaches 4″ plate (Chomérat et al., 2020), which contradicts the original description by Quod (1994). All these findings suggest the actual shape of this plate was probably overlooked in previous studies. In *O.*

siamensis, Fukuyo (1981) interpreted a small, long and narrow 2′ plate as reported in the original drawing by Schmidt (1901), but the exact shape and length are not clearly visible from LM pictures. So whether the 2′ plate was actually short in the population or the interpretation was influenced by the original description could not be determined. As previously emphasized by Chomérat et al. (2020), the study of this plate is extremely difficult due to its narrowness and recessed position below the APC. The relevance of this plate has also significantly increased with the descriptions of new *Ostreopsis* species characterized by rather close plate pattern. Indeed, the need to identify consistent diagnostic features and the development of more and more powerful techniques such as epifluorescence or SEM has rendered the study of the APC and 2′ plate more prominent in modern taxonomy. When Schmidt (1901) described *O. siamensis*, the morphology of this new genus was so unusual and different from all other known dinoflagellates, that there was probably no need to study this tiny and recessed plate with as many details as today, therefore original drawings should be taken cautiously. To support this statement, it should be mentioned that Schiller even omitted to report the APC and 2′ plate in the illustration of the genus *Ostreopsis* in his monograph (Fig. 543b in Schiller, 1937).

All the above morphological features reported for the specimens from Tahiti are in rather good agreement with the description of *O. siamensis*, and the fact that it is genetically almost identical to a strain from the type locality strongly argues in favor of this identity. Nevertheless, most of these features fit also quite well with the description of another species, *O. labens* which also has a conspicuous undulation and is very difficult to separate from *O. siamensis*. The type locality of *O. labens* is Man of war Cay, Belize but Faust and Morton (1995) indicated the presence of this species in several places from Japan (Iriomote, Ishigaki Islands) and East China, and this distribution was extended to southwestern Indian Ocean (Faust et al., 1996). The reasons why *O. labens* has been separated from *O. siamensis* are unclear, and the main difference between them appears to be the anteroposterior length reported as 60–86 µm in *O. labens* (Faust and Morton, 1995), which is higher

than for *O. siamensis* (Hoppenrath et al., 2014). Nevertheless, this feature is doubtful since it does not correspond to the illustrations provided by Faust and Morton (1995) and based on the scale bar, the cell illustrated in their Fig. 8 had an estimated width of 67 µm and an AP length of 44 µm, which is surprisingly outside the range given in the description. Hence, the diagnostic features of *O. labens* appear to be questionable, and the dimensions must be regarded cautiously. In their description of *O. labens*, Faust and Morton (1995) reported a DV length (depth) of 81–110 µm but this was surprisingly further reported to 86–98 µm one year later (Faust et al., 1996). Thus, it is mostly in the range given by Fukuyo (1981) for *O. siamensis* (60–100 µm). Moreover, as discussed earlier, Faust et al. (1996) likely made a major confusion between *O. siamensis* and *O. lenticularis* and all their data reported for '*O. lenticularis*' (our quotation marks) actually fit better with *O. siamensis,* while the data for '*O. siamensis*' concern *O. lenticularis* (Chomérat et al., 2019). According to Faust et al. (1996), '*O. lenticularis*' (likely *O. siamensis*) has a DV length of 65–75 µm which is not only in the range given by Fukuyo (1981) for *O. siamensis* but also in the range of *Ostreopsis* sp. 6 [strain TF29OS (Tawong et al., 2014) and field cells observed in the present study]. Unfortunately, Faust et al. (1996) did not report the AP length for this species, preventing any further comparison with *O. labens*. Except for size, no striking difference can be found between *O. labens* and '*O. lenticularis*' (likely *O. siamensis*) in Faust et al. (1996). They both possess a similar thecal arrangement, an undulated cingulum (undescribed but visible on the illustrations), and large thecal pores in depressions and surrounded with a rim (Faust et al., 1996). This structure of large thecal pores is remarkably similar in *Ostreopsis* sp. 6 (*e.g.*, Fig. 29 in Fukuyo, 1981; Fig. 2H in Lee and Park, 2020, present study), *O. labens* and *'O. lenticularis'* (Faust and Morton, 1995; Faust et al., 1996), indicating their probable taxonomic proximity and possible conspecificity. The presence of very small thecal pores observed in the present study may have been overlooked in older studies since these pores are rare on the cell surface and they require that the amphiesmal and cell

membranes to be well removed. In any case, these small pores are impossible to see in LM, and their scarcity on thecal plates makes a major difference from *O. lenticularis* (Chomérat et al., 2019).

In the light of the molecular data showing that *Ostreopsis* sp. 6 encompasses cryptic diversity, one of the subclades D or E might correspond to *O. labens* since Faust and Morton (1995) designated paratypes from Iriomote and Ishigaki islands, Japan. Phylogenetic analyses revealed that great diversity exists at Iriomote-Kohama-Ishikagi Islands which are part of the Ryukyu archipelago, and sequences clustering in the subclades D and E are both present. Since Fukuyo (1981) studied specimens from this area, he may have reinterpreted *O. siamensis* in a broad sense, encompassing cryptic (or pseudocryptic) species within *Ostreopsis* sp. 6, and possibly *O. labens*. However, to confirm this hypothesis and clarify the delineation of *O. labens*, additional molecular data are needed from the type locality (Man of war Cay, Belize).

The molecular data from the Gulf of Thailand and type locality of *O. siamensis* (Tawong et al. 2014), together with the detailed morphological description herein bring new evidence that the subclades A and B of *Ostreopsis* sp. 6 likely correspond to the real *Ostreopsis siamensis,* as described by Schmidt (1901). Nevertheless, in the absence of a culture of this species from the type locality in the Gulf of Thailand, it is impossible to define a neotype yet. In contrast with the recent review by Tester et al. (2020), this study demonstrates unambiguously that *Ostreopsis* sp. 6 should not be considered as a cryptic species of *O. lenticularis* (= *Ostreopsis* sp. 5), and instead, corresponds to a fully separated species, most likely *O. siamensis*. This novel report from Tahiti Island is extremely interesting as only two morphospecies are currently reported from French Polynesia so far, namely *O. ovata* and *O. lenticularis* (Fukuyo, 1981; Chomérat et al., 2019). In his study, Fukuyo (1981) clearly indicated that *O. siamensis* was not present in the samples from Tahiti and Gambier Islands.

4.1.3 Taxonomic comparison with 'Ostreopsis *cf.* siamensis*' from temperate locations*

The nomenclatural combination '*Ostreopsis* cf. *siamensis"* has been used to designate a clade that includes sequences from the Mediterranean, Atlantic-Iberian peninsula, northern New Zealand, Russia and Australia which all classify in temperate (Cf) to warm Mediterranean climates (Csa) and subtropical humid (Cwa) according to the Köppen-Geiger climatic classification (Table 3, Peel et al., 2007; Beck et al., 2018). In contrast with *Ostreopsis* sp. 6 for which genetic divergence is relatively high and may indicate the existence of cryptic species, molecular data for '*O.* cf. *siamensis*' show a lower level of variation among populations from the different temperate areas. Hence '*O.* cf. *siamensis*' can be interpreted as a single species, related to *O. rhodesiae* in phylogenies, but very recently, Verma et al. (2020) showed the existence of low genetic variability and identified two subclades within '*O.* cf. *siamensis'* from Australia. Despite this relative genetic stability, morphology reported for this species is rather variable and sometimes conflicting features have been mentioned but it is likely that several confusions were made and the taxonomic identity was not ascertained. The lack of molecular data for previous reports from the temperate areas (*e.g.*, the northern part of New Zealand, Chang et al., 2000; Rhodes et al., 2000) prevents to clarify their actual identity and morphological data were not detailed enough to conclude. Nevertheless, it is likely the same temperate species that clusters in the clade '*O.* cf. *siamensis*' since it was found in the northern part of New Zealand for which genetic data have been further acquired (Sato et al., 2011). In contrast, the species identified morphologically as *Ostreopsis* cf. *siamensis* by Holmes et al. (1988) from subtropical Australia (Heron and Lady Elliot islands) likely correspond to another taxon, presumably *O. siamensis*, as shown by size and characters (Table 3). Although the presence of '*O.* cf. *siamensis*' has also recently been confirmed at Heron Island (Verma et al., 2016a) the cells had different morphological characters (Table 3). In this area of Coral Sea, which is corresponds to the limit of the tropical area, both genotypes may be sympatric. Hence, it appears that the

combination '*Ostreopsis* cf. *siamensis"* may have been used for different taxa and is highly confusing.

As summarized by Verma et al. (2016b), the sizes reported for temperate specimens (excluding all reports from tropical waters that likely correspond to other species, Table 3) were quite variable, depending on whether observations used cultured material or field fixed specimens. The DV length varied between 34 µm (*e.g.,* cultured cells from Merimbula, Australia, Verma et al., 2016b), to 90 µm (*e.g.*, field specimens from the Mediterranean Sea, Penna et al., 2005). This suggests that size is a poor taxonomical character to distinguish temperate '*O.* cf. *siamensis'* from tropical *O. siamensis* and *Ostreopsis* sp. 6 due to the overlap (Table 3). Besides, as for almost all *Ostreopsis* species, the plate pattern does not exhibit any major difference (Parsons et al., 2012). Interestingly, in their Fig. 2f, Verma et al. (2016b) illustrated a short 2′ plate, not reaching the precingular 4″ plate, very similar to Schmidt's illustration, but their SEM micrograph of the 2′ plate (cf. Fig. 3c in Verma et al., 2016b) is not clear and seems to indicate a contact between 2′ and 4″ plates. In contrast, Selina and Orlova (2010) and David et al. (2013) illustrated a conspicuously long 2′ plate, as shown in our study. Consequently, the length of 2′ plate does not constitute a good character to distinguish '*O.* cf. *siamensis'* from *Ostreopsis* sp. 6 and it appears necessary to reinvestigate this feature for all *Ostreopsis* species as the interpretation may have been mistaken.

Two important features should be better evaluated for the discrimination of species from the tropical area (*O. siamensis* / *O. labens*/ *Ostreopsis* sp. 6) from the more temperate '*O.* cf. *siamensis*'. The first feature seems to be the cingulum undulation, which is conspicuous in the original description of *O. siamensis* and the present study of *Ostreopsis* sp. 6. As shown in Table 3, when studied carefully, the conspicuous undulation is found in tropical populations of *O. siamensis*, *O. labens,* and *Ostreopsis* sp. 6 whereas in populations of '*O.* cf *siamensis*', this feature has been rarely emphasized. Several authors indicated that cells were flat and not undulated (Penna et al., 2005; David et al., 2013; Verma et al., 2016b) while Aligizaki and Nikolaidis (2006) reported that

653 cells were sometimes undulated. The undulation showed in Fig. 4A by Aligizaki and Nikolaidis
654 (2006) appears very faint and roughly similar to the observations by Selina and Orlova (2010).
655 Nevertheless, in these studies, the illustrations do not show the same degree of undulation as
656 illustrated by Schmidt (1901) or shown in the present study. Consequently, the degree of undulation
657 may constitute a good feature to separate temperate '*O.* cf. *siamensis*' from the tropical *O. siamensis*
658 / *Ostreopsis* sp. 6. Additionally, thecal pores may constitute another important taxonomic feature, to
659 help separate these taxa. As shown in Table 3, the size of large and small thecal pores may be an
660 interesting feature to consider, although this is variable among populations. It is striking that large
661 thecal pores have the same size in *Ostreopsis* sp. 6 from the Gulf of Thailand (Tawong et al., 2014)
662 and Tahiti (this study). This large size (0.4–0.7 µm) compares well with Schmidt's statement that
663 plates are coarsely porous, like that of '*Ceratium tripos*' (Schmidt, 1901), who observed them only
664 with LM. From the original drawings (cf. Fig. 6 in Schmidt, 1901), the thecal pores illustrated on
665 the hypotheca have a roughly estimated size of 0.6–0.7 µm, considering the DV length of the cells
666 *ca.* 90 µm. As observed in the present study, rounded cells were generally much smaller, and in
667 absence of a scale bar in the original description, the pores size could not be estimated from the
668 epitheca (Fig. 5 in Schmidt, 1901), or some exceed 1 µm if the DV is considered to be 90 µm. By
669 contrast, the values for '*O.* cf. *siamensis*' appear lower in all studies. Penna et al. (2005) made
670 extensive measurements of thecal pores of *O.* cf. *siamensis* from the Mediterranean Sea, but despite
671 a large range of variation of 0.11–0.55 µm, the predominant size was 0.2–0.4 µm which is below
672 the measurements in *Ostreopsis* sp. 6 (Tawong et al., 2014; this study). In addition to the size, the
673 structure of these pores, with a depression and collar rim around the opening appears conspicuous in
674 *Ostreopsis* sp. 6, but it has never been shown in the temperate '*O.* cf. *siamensis*' which has simple
675 pores without collar rim. Thus, this feature should be further considered to separate these species.

676 Therefore, in the light of the phylogenetic data presently available and the morphological data
677 from the present study, we conclude the name *O. siamensis* should be used for a species within the

678 clade *Ostreopsis* sp. 6 (putatively the subclades A and B), while there is a need to rename '*O.* cf.
679 *siamensis*' from temperate areas since this designation is a source of additional confusion in the
680 complex taxonomy of *Ostreopsis.*

681

682 *4.2 Toxicity and toxin profiles*

683 As previously found by Pawlowiez et al. (2013), Cañete and Diogène (2008) and Kerbrat et al.
684 (2011), the cytotoxic effect of PlTX on N2a cells was enhanced by the presence of ouabain which is
685 in marked contrast with Ledreux et al. (2009) who concluded in a protective effect of ouabain
686 against PlTX action. In French Polynesia, the composite toxicity detected by CBA-N2a showed that
687 all the strains isolated from the bloom were toxic in O^- and O^+ conditions with a mean production of
688 at least 1.27 pg PlTX equiv. $cell^{-1}$ estimated in O^+ condition and very little difference between the
689 eight strains (9.2%). This composite toxicity was confirmed by LC-MS/MS analyses revealing the
690 presence of three OST analogs in all strains of *Ostreopsis* sp. 6 from Tahiti: OST-A, OST-B, and
691 OST-D, this latter composing the most important part of the toxin profile (≈ 90%). The average
692 toxin production of the eight strains as assessed by LC-MS/MS was estimated at 25 pg equiv. PlTX
693 $cell^{-1}$ i.e. 19-fold higher than with the CBA-N2a. This bias could be explained by the use of PlTX as
694 the reference standard to estimate the toxin production (since OST standards are currently
695 unavailable). The use of PlTX could not allow estimating the real cytotoxic potential of these three
696 OSTs (-A, -B and -D) on mouse neuroblastoma cells via the CBA-N2a, as-yet-unknown. Depending
697 on the model and exposition routes, considerable differences have been found between PlTX and
698 OST-D (Ito and Yasumoto, 2009). For instance, *in vivo* experiments on mice (intra-tracheal
699 administration) have shown that OST-D was five times less potent than PlTX (Ito and Yasumoto,
700 2009). Using keratinocytes (HaCaT cells), Pelin et al. (2016) also noticed a lesser cytotoxicity of
701 OST-D in comparison with PlTX, and suggested that a missing hydroxyl group on C44 of OST-D,
702 present in PlTX, may cause this major difference in toxicity.

703 In previous studies, crude methanolic extracts of the strain s0587 (subclade D) from Haemida,
704 South of Iriomote Island (latitude ≈24°N), in tropical waters of Okinawa, Japan (Sato et al., 2011)
705 and the strain TF29OS (subclade B) from Thailand (Tawong et al., 2014) belonging to *Ostreopsis*
706 sp. 6 and genetically closely related to the strains from Tahiti, exhibited toxicity to mice although no
707 quantification was given. The same strain s0587 was also known to produce OST-D, around 3.5 pg
708 PlTX equiv. cell-1 (Suzuki et al., 2012) using LC-MS/MS, which is *ca.* 7 times lower than for the
709 French Polynesian strains. These levels are rather similar, albeit lower compared to other *Ostreopsis*
710 species like *O.* cf. *ovata* from the northern Adriatic Sea showing high levels of PlTXs up to 75 pg
711 $cell^{-1}$ in natural benthic microalgal populations (Accoroni et al., 2011). Interestingly, Suzuki et al.
712 (2012) did not detect any toxins in strains IR33 and OU11 (subclade E) of *Ostreopsis* sp. 6, which
713 contrasts with subclades A, B and D.

714 Regarding the toxin profiles, the presence of OST-D as the major analogue found in the strains
715 from French Polynesia (this study) is consistent with results obtained previously for Japanese
716 strains, including the strain s0587 (Suzuki et al., 2012), but also with the data by Ukena et al. (2001,
717 2002) who isolated and purified OST-D from the strain SOA1, collected at Aka Island, Okinawa,
718 Japan. In addition, the presence of at least three analogues within a single strain is also consistent
719 with the recent studies of Terajima et al. (2018a, b) who purified the four OSTs known so far from
720 the same SOA1 strain. Although this strain comes from the same island than strain OA21 (subclade
721 D/E? in Fig. 7), no sequence has been provided for strain SOA1 which prevents a genetic
722 comparison. Phylogenetic data suggest that there is a great diversity in the area of Iriomote-
723 Kohama-Okinawa islands, including several genotypes of *Ostreopsis* sp. 6 (Sato et al., 2011; this
724 study). In all phylogenetic analyses, sequences from Japan do not cluster in the same subclade as
725 those from the Gulf of Thailand and Tahiti, which could indicate different species. Further work
726 will thus be needed to clarify this and ascertain the presence of OST-E1 in strains from Tahiti. To
727 date, the lack of published profiles limits further comparisons of the toxin profile found for

728 *Ostreopsis* sp. 6. Nonetheless, results obtained in this study clearly indicate that comparing toxicity
729 and toxin composition of tropical strains of *Ostreopsis* sp. 6 with temperate strains of '*O.* cf.
730 *siamensis*' (*e.g.*, Tester et al., 2020) should be very cautious since they concern two widely
731 divergent taxa. Such apparent conflicting reports of toxicity may result from misidentifications, and
732 we recommend that future works on toxicity always include a molecular characterization of the
733 strains studied to ensure their correct identification.

734 While all the strains isolated from the bloom exhibited toxicity, the absence of noticeable
735 toxicity and no detection of toxins from the field sample raises questions. Since the observations of
736 the bloom sample showed that several diatoms were co-occurring with *Ostreopsis* sp. 6, it is likely
737 that the dried biomass represented by *Ostreopsis* cells was rather low and probably insufficient to
738 induce a cytotoxic effect and to detect toxins. In addition, it has been shown that toxicity is highly
739 dependent on the bloom dynamics, and Gémin et al. (2020) reported that the toxin content increased
740 during the exponential and stationary growth phases of a bloom of *O.* cf. *ovata*. Hence, the toxin
741 content per cell in the bloom at Toaroto beach could have been low if sampling was done at an early
742 stage. In any case, further investigations will be necessary to confirm such findings, both *in situ* and
743 in laboratory conditions, as this has major implications in terms of risk in a given area.

744

745 **5. Conclusions**

746 In the context of climate change and global warming, understanding the ecological preferences
747 and niche of harmful benthic microalgae is an important challenge in order to predict future changes
748 (Tester et al., 2020). Among these taxa, the genus *Ostreopsis* represents a serious threat since
749 several species are toxic not only to human but also to marine organisms. The present observation
750 of a bloom of *Ostreopsis* sp. 6 in French Polynesia constitutes a new record for this species since, to
751 date, only *O. ovata* and *O. lenticularis* have been mentioned from French Polynesia (Fukuyo, 1981;

752 Bagnis et al., 1985; Chomérat et al., 2019). Hence, the finding of a new, toxic species, in Tahiti
753 increases the potential risk linked to the proliferation of *Ostreopsis*. The fact that no toxicity was
754 found in environmental samples whereas all clonal strains established from the bloom were toxic
755 with a relatively similar profile, dominated by OST-D, raises important questions about the basis of
756 toxin production in this species. While *O.* cf. *ovata* is likely the most toxic species, the risk to
757 human populations in the Mediterranean seems manageable, but the situation may be very different
758 in tropical areas (Tester et al., 2020). As emphasized by Deeds and Schwartz (2010), PlTX-like
759 molecules may accumulate and contaminate tropical fishes and their ingestion by humans can have
760 dramatic health impacts, in addition to the well-known risk of CFP. Hence, further studies aiming at
761 better evaluate the distribution of *Ostreopsis* sp. 6 in French Polynesia, and determine the ecological
762 conditions which stimulates its proliferation now appear crucial for a better assessment of its
763 potential impacts on the coral-reef ecosystems but also risk management purposes.

764

765 **6. ACKNOWLEDGEMENTS**

766 We thank Maurice Loir for his help in the identification of the diatoms co-occurring with the
767 *Ostreopsis* bloom and Frederic Zentz for designing the new primer Dino-RB. The four anonymous
768 reviewers are acknowledged for their suggestions improving significantly the manuscript. The
769 Regional Council of Brittany, the General Council of Finistère and the urban community of
770 Concarneau-Cornouaille-Agglomération are acknowledged for the funding of the Sigma 300 FE-
771 SEM of the station of Marine Biology in Concarneau.

772

Funding

This work is part of the TATOO project and was supported by funds from the Délégation à la Recherche de la Polynésie Française (Conv. n°02400/MTF/REC of April 9th, 2018).

Authors contributions

Conceptualization : NC, MC

– Field sampling : MZ, CV, AU, KH

– Microscopy observations : NC, KH

– *in vitro* culturing : KH

– Acquisition and analysis of molecular data : NC, GB

– Acquisition and analysis of toxicity data (including extraction steps) : JV, FH, DR, AD, ZA, HTD, MR

– Writing—original draft preparation : NC, HTD, DR, MC

– Writing—review and editing : NC, GB, JV, FH, DR, MZ, CV, CG, MR, HTD, MC

– Project supervision : MC, NC

– Funding acquisition : MC, NC

789 **References**

790 Accoroni, S., Romagnoli, T., Colombo, F., Pennesi, C., Di Camillo, C.G., Marini, M., Battocchi, C.,
791 Ciminiello, P., Dell'Aversano, C., Dello Iacovo, E., Fattorusso, E., Tartaglione, L., Penna,
792 A., Totti, C., 2011. *Ostreopsis* cf. *ovata* bloom in the northern Adriatic Sea during summer
793 2009: Ecology, molecular characterization and toxin profile. Mar. Pollut. Bull. 62, 2512–
794 2519. https://doi.org/10.1016/j.marpolbul.2011.08.003
795 Accoroni, S., Totti, C., 2016. The toxic benthic dinoflagellates of the genus *Ostreopsis* in temperate
796 areas: a review. Adv. Oceanogr. Limnol. 7, 1–15. https://doi.org/10.4081/aiol.2016.5591
797 Accoroni, S., Romagnoli, T., Penna, A., Capellacci, S., Ciminiello, P., Dell'Aversano, C.,
798 Tartaglione, L., Abboud-Abi Saab, M., Giussani, V., Asnaghi, V., Chiantore, M., Totti, C.,
799 2016. *Ostreopsis fattorussoi* sp. nov. (Dinophyceae), a new benthic toxic *Ostreopsis* species
800 from the eastern Mediterranean Sea. J. Phycol. 52, 1064–1084.
801 https://doi.org/10.1111/jpy.12464
802 Alcala, A.C., Alcala, L.C., Garth, J.S., Yasumura, D., Yasumoto, T., 1988. Human fatality due to
803 ingestion of the crab *Demania reynaudii* that contained a palytoxin-like toxin. Toxicon 26,
804 105–107.
805 Aligizaki, K., Nikolaidis, G., 2006. The presence of the potentially toxic genera *Ostreopsis* and
806 *Coolia* (Dinophyceae) in the North Aegean Sea, Greece. Harmful Algae 5, 717–730.
807 https://doi.org/10.1016/j.hal.2006.02.005
808 Amzil, Z., Sibat, M., Chomérat, N., Grossel, H., Marco-Miralles, F., Lemée, R., Nézan, E., Séchet,
809 V., 2012. Ovatoxin-a and Palytoxin Accumulation in seafood in relation to *Ostreopsis* cf.
810 *ovata* blooms on the French Mediterranean coast. Mar. Drugs 10, 477–496.
811 Bagnis, R., Bennett, J., Prieur, C., Legrand, A.-M., 1985. The dynamics of three toxic benthic
812 dinoflagellates and the toxicity of ciguateric surgeonfish in French Polynesia, in: Anderson,
813 D.M., White, A.W., Baden, D.G. (Eds.), Toxic Dinoflagellates. Proceedings of the Third

International Conference on Toxic Dinoflagellates. Presented at the Third International Conference on Toxic Dinoflagellates, Elsevier, New York, St. Andrews, New Brunswick, Canada, pp. 177–182.

Ballantine, D., L., Tosteson, T.R., Bardales, A.T., 1988. Population dynamics and toxicity of natural populations of benthic dinoflagellates in southwestern Puerto Rico. J. Exp. Mar. Biol. Ecol. 119, 201–212.

Beck, H.E., Zimmermann, N.E., McVicar, T.R., Vergopolan, N., Berg, A., Wood, E.F., 2018. Present and future Köppen-Geiger climate classification maps at 1-km resolution. Sci. Data 5, 180214. https://doi.org/10.1038/sdata.2018.214

Berdalet, E., Chinain, M., Fraga, S., Lemée, R., Litaker, W., Penna, A., Usup, G., Vila, M., Zingone, A., 2017. Harmful Algal Blooms in Benthic Systems: Recent Progress and Future Research. Oceanography 30, 36–45. https://doi.org/10.5670/oceanog.2017.108

Besada, E.G., Loeblich, L.A., Loeblich, A.R., III, 1982. Observations on tropical, benthic dinoflagellates from ciguatera-endemic areas: *Coolia, Gambierdiscus* and *Ostreopsis*. Bull. Mar. Sci. 32, 723–735.

Brissard, C., Herrenknecht, C., Séchet, V., Hervé, F., Pisapia, F., Harcouet, J., Lemée, R., Chomérat, N., Hess, P., Amzil, Z., 2014. Complex toxin profile of French Mediterranean *Ostreopsis* cf. *ovata* strains, seafood accumulation and ovatoxins prepurification. Mar. Drugs 12, 2851–2876.

Cañete, E., Diogène, J., 2008. Comparative study of the use of neuroblastoma cells (Neuro-2a) and neuroblastoma×glioma hybrid cells (NG108-15) for the toxic effect quantification of marine toxins. Toxicon 52, 541–550. https://doi.org/10.1016/j.toxicon.2008.06.028

Carlson, R.D., Tindall, D.R., 1985. Distribution and periodicity of toxic dinoflagellates in the Virgin Islands, in: Anderson, D.M., White, A.W., Baden, D.G. (Eds.), Toxic Dinoflagellates. Proceedings of the Third International Conference on Toxic Dinoflagellates. Presented at the

839 International Conference on Toxic Dinoflagellates, Elsevier, New York, St. Andrews, New
840 Brunswick, Canada, pp. 171–176.
841 Chang, F.H., Shimizu, Y., Hay, B., Stewart, R., Mackay, G., Tasker, R., 2000. Three recently
842 recorded *Ostreopsis* spp. (Dinophyceae) in the New Zealand: temporal and regional
843 distribution in the upper North Island from 1995 to 1997. N. Z. J. Mar. Freshw. Res. 34, 29–
844 39.
845 Chinain, M., Darius, H.T., Gatti, C.M., Roué, M., 2016. Update on ciguatera research in French
846 Polynesia. SPC Fish. Newsl. 150, 42–51.
847 Chinain, M., Gatti, C.M., Roué, M., Darius, H.T., 2020. Ciguatera_causing dinoflagellates in the
848 genera *Gambierdiscus* and *Fukuyoa*: Distribution, ecophysiology and toxicology, in: Subba
849 Rao, D.V. (Ed.), Dinoflagellates: Morphology, Life-History and Ecological Significance.
850 Nova Science Publishers, New-York, 66 pp.
851 Chomérat, N., Couté, A., 2008. *Protoperidinium bolmonense* sp. nov. (Peridiniales, Dinophyceae), a
852 small dinoflagellate from a brackish hypereutrophic lagoon (South of France). Phycologia
853 47, 392–403.
854 Chomérat, N., Mahana iti Gatti, C., Nézan, E., Chinain, M., 2017. Studies on the benthic genus
855 *Sinophysis* (Dinophysales, Dinophyceae) II. *S. canaliculata* from Rapa Island (French
856 Polynesia). Phycologia 56, 193–203.
857 Chomérat, N., Bilien, G., Derrien, A., Henry, K., Ung, A., Viallon, J., Darius, H.T., Mahana iti Gatti,
858 C., Roué, M., Hervé, F., Réveillon, D., Amzil, Z., Chinain, M., 2019. *Ostreopsis lenticularis*
859 Y. Fukuyo (Dinophyceae, Gonyaulacales) from French Polynesia (South Pacific Ocean): A
860 revisit of its morphology, molecular phylogeny and toxicity. Harmful Algae 84, 95–111.
861 https://doi.org/10.1016/j.hal.2019.02.004
862 Chomérat, N., Bilien, G., Couté, A., Quod, J.-P., 2020. Reinvestigation of *Ostreopsis mascarenensis*
863 Quod (Dinophyceae, Gonyaulacales) from Réunion Island (SW Indian Ocean): molecular

phylogeny and emended description. Phycologia 1–14. https://doi.org/10.1080/00318884.2019.1710443

Ciminiello, P., Dell'Aversano, C., Fattorusso, E., Forino, M., Tartaglione, L., Grillo, C., Melchiorre, N., 2008. Putative palytoxin and its new analogue, ovatoxin-a, in *Ostreopsis ovata* collected along the ligurian coasts during the 2006 toxic outbreak. J. Am. Soc. Mass Spectrom. 19, 111–120. https://doi.org/10.1016/j.jasms.2007.11.001

Ciminiello, P., Dell'Aversano, C., Iacovo, E.D., Fattorusso, E., Forino, M., Tartaglione, L., Yasumoto, T., Battocchi, C., Giacobbe, M., Amorim, A., Penna, A., 2013. Investigation of toxin profile of Mediterranean and Atlantic strains of *Ostreopsis* cf. *siamensis* (Dinophyceae) by liquid chromatography–high resolution mass spectrometry. Harmful Algae 23, 19–27. https://doi.org/10.1016/j.hal.2012.12.002

Ciminiello, P., Dell'Aversano, C., Iacovo, E.D., Fattorusso, E., Forino, M., Tartaglione, L., Benedettini, G., Onorari, M., Serena, F., Battocchi, C., Casabianca, S., Penna, A., 2014. First finding of *Ostreopsis* cf. *ovata* toxins in marine aerosols. Environ. Sci. Technol. 48, 3532–3540. https://doi.org/10.1021/es405617d

Cohu, S., Thibaut, T., Mangialajo, L., Labat, J.P., Passafiume, O., Blanfune, A., Simon, N., Cottalorda, J.M., Lemee, R., 2011. Occurrence of the toxic dinoflagellate *Ostreopsis* cf. *ovata* in relation with environmental factors in Monaco (NW Mediterranean). Mar Pollut Bull 62, 2681–91. https://doi.org/10.1016/j.marpolbul.2011.09.022

Darius, H.T., Roué, M., Sibat, M., Viallon, J., Gatti, C.M. iti, Vandersea, M.W., Tester, P.A., Litaker, R.W., Amzil, Z., Hess, P., Chinain, M., 2018. Toxicological investigations on the sea urchin *Tripneustes gratilla* (Toxopneustidae, Echinoid) from Anaho Bay (Nuku Hiva, French Polynesia): Evidence for the presence of Pacific ciguatoxins. Mar. Drugs 16, 122. https://doi.org/10.3390/md16040122

888 Darriba, D., Taboada, G.L., Doallo, R., Posada, D., 2012. jModelTest 2: more models, new
889 heuristics and parallel computing. Nat. Methods 9, 772. https://doi.org/10.1038/nmeth.2109
890 David, H., Laza-Martínez, A., Miguel, I., Orive, E., 2013. *Ostreopsis* cf. *siamensis* and *Ostreopsis*
891 cf. *ovata* from the Atlantic Iberian Peninsula: Morphological and phylogenetic
892 characterization. Harmful Algae 30, 44–55. https://doi.org/10.1016/j.hal.2013.08.006
893 Deeds, J.R., Schwartz, M.D., 2010. Human risk associated with palytoxin exposure. Toxicon 56,
894 150–162. https://doi.org/10.1016/j.toxicon.2009.05.035
895 Faust, M.A., Morton, S.L., 1995. Morphology and ecology of the marine dinoflagellate *Ostreopsis*
896 *labens* sp. nov. (Dinophyceae). J. Phycol. 31, 456–463.
897 Faust, M.A., Morton, S.L., Quod, J.-P., 1996. Further SEM study of marine dinoflagellates: the
898 genus *Ostreopsis* (Dinophyceae). J. Phycol. 32, 1053–1065.
899 Ferreira, C.E.L., 2006. Sea urchins killed by toxic algae. JMBA Glob. Mar Env. 3, 23–24.
900 Fukuyo, Y., 1981. Taxonomical study on benthic dinoflagellates collected in coral reefs. Bull. Jpn.
901 Soc. Sci. Fish. 47, 967–978.
902 Gémin, M.-P., Réveillon, D., Hervé, F., Pavaux, A.-S., Tharaud, M., Séchet, V., Bertrand, S., Lemée,
903 R., Amzil, Z., 2020. Toxin content of *Ostreopsis* cf. *ovata* depends on bloom phases, depth
904 and macroalgal substrate in the NW Mediterranean Sea. Harmful Algae 92, 101727.
905 https://doi.org/10.1016/j.hal.2019.101727
906 GEOHAB, 2012. Global Ecology and Oceanography of Harmful Algal Blooms, GEOHAB Core
907 Research Project: HABs in Benthic Systems. Berdalet E., Tester P. and Zingone A. (Eds.).
908 IOC of UNESCO and SCOR, Paris and Newark.
909 Georges des Aulnois, M., Roux, P., Caruana, A., Réveillon, D., Briand, E., Hervé, F., Savar, V.,
910 Bormans, M., Amzil, Z., 2019. Physiological and metabolic responses of freshwater and
911 brackish-water strains of *Microcystis aeruginosa* acclimated to a salinity gradient: insight

912 into salt tolerance. Appl. Environ. Microbiol. 85, e01614-19, /aem/85/21/AEM.01614-
913 19.atom. https://doi.org/10.1128/AEM.01614-19
914 Guidi-Guilvard, L.D., Gasparini, S., Lemée, R., 2012. The Negative Impact of *Ostreopsis* cf. *Ovata*
915 on Phytal Meiofauna from the Coastal NW Mediterranean. Cryptogam. Algol. 33, 121–128.
916 https://doi.org/10.7872/crya.v33.iss2.2011.121
917 Guindon, S., Dufayard, J.-F., Lefort, V., Anisimova, M., Hordijk, W., Gascuel, O., 2010. New
918 algorithms and methods to estimate Maximum-Likelihood phylogenies: assessing the
919 performance of PhyML 3.0. Syst. Biol. 59, 307–21.
920 Holmes, M.J., Gillespie, N.C., Lewis, R.J., 1988. Toxicity and morphology of *Ostreopsis* cf.
921 *siamensis* cultured from a ciguatera endemic region of Queenland, Australia, in: Choat, J.H.,
922 Barnes, D., Borowitzka, M.A., Coll, J.C., Davies, P.J., Flood, P., Hatcher, B.G., Hopley, D.,
923 Hutchings, P.A., Kinsey, D., Orme, G.R., Pichon, M., Sale, P.F., Sammarco, P., Wallace,
924 C.C., Wilkinson, C., Wolanski, E., Bellwood, O. (Eds.), Proceedings of the 6th International
925 Coral Reef Symposium, Vol. 3. Townsville, Australia, pp. 49–54.
926 Holmes, M.J., Lewis, R.J., Poli, M.A., Gillespie, N.C., 1991. Strain dependent production of
927 ciguatoxin precursors (gambiertoxins) by *Gambierdiscus toxicus* (Dinophyceae) in culture.
928 Toxicon 29, 761–775. https://doi.org/10.1016/0041-0101(91)90068-3
929 Hoppenrath, M., Murray, S., Chomérat, N., Horiguchi, T., 2014. Marine benthic dinoflagellates -
930 unveiling their worldwide biodiversity (Kleine Senckenberg-Reihe 54). E.
931 Schweizerbart'sche Verlagbuchhandlung.
932 Ito, E., Yasumoto, T., 2009. Toxicological studies on palytoxin and ostreocin-D administered to
933 mice by three different routes. Toxicon 54, 244–251.
934 https://doi.org/10.1016/j.toxicon.2009.04.009

935 Katoh, K., Standley, D.M., 2013. MAFFT multiple sequence alignment software version 7:
936 improvements in performance and usability. Mol. Biol. Evol. 30, 772–80.
937 https://doi.org/10.1093/molbev/mst010
938 Kerbrat, A.S., Amzil, Z., Pawlowiez, R., Golubic, S., Sibat, M., Darius, H.T., Chinain, M., Laurent,
939 D., 2011. First evidence of palytoxin and 42-hydroxy-palytoxin in the marine
940 cyanobacterium *Trichodesmium*. Mar. Drugs 9, 543–560.
941 https://doi.org/10.3390/md9040543
942 Kumar, S., Stecher, G., Li, M., Knyaz, C., Tamura, K., 2018. MEGA X: Molecular Evolutionary
943 Genetics Analysis across Computing Platforms. Mol. Biol. Evol. 35, 1547–1549.
944 https://doi.org/10.1093/molbev/msy096
945 Laza-Martínez, A., Orive, E., Irati, M., 2011. Morphological and genetic characterization of benthic
946 dinoflagellates of the genera *Coolia*, *Ostreopsis* and *Prorocentrum* from south-eastern Bay
947 of Biscay. Eur. J. Phycol. 46, 45–65.
948 Leaw, C.P., Lim, P.T., Asmat, A., Usup, G., 2001. Genetic Diversity of *Ostreopsis ovata*
949 (Dinophyceae) from Malaysia. Marine Biotechnology 3, 246–255.
950 https://doi.org/10.1007/s101260000073
951 Ledreux, A., Krys, S., Bernard, C., 2009. Suitability of the Neuro-2a cell line for the detection of
952 palytoxin and analogues (neurotoxic phycotoxins). Toxicon 53, 300–308.
953 https://doi.org/10.1016/j.toxicon.2008.12.005
954 Lee, B., Park, M.G., 2020. Distribution and genetic diversity of the toxic benthic dinoflagellate
955 genus *Ostreopsis* in Korea. Harmful Algae 96, 101820.
956 https://doi.org/10.1016/j.hal.2020.101820
957 Litaker, R.W., Vandersea, M.W., Kibler, S.R., Reece, K.S., Stokes, N.A., Lutzoni, F.M., Yonish,
958 B.A., West, M.A., Black, M.N.D., Tester, P.A., 2007. Recognizing dinoflagellates using ITS
959 rDNA sequences. J. Phycol. 43, 344–355.

960 Mangialajo, L., Bertolotto, R., Cattaneo-Vietti, R., Chiantore, M., Grillo, C., Lemee, R., Melchiorre,
961 N., Moretto, P., Povero, P., Ruggieri, N., 2008. The toxic benthic dinoflagellate *Ostreopsis*
962 *ovata*: Quantification of proliferation along the coastline of Genoa, Italy. Mar. Pollut. Bull.
963 56, 1209–1214. https://doi.org/10.1016/j.marpolbul.2008.02.028
964 Moore, R.E., Scheuer, P.J., 1971. Palytoxin: a new marine toxin from a Coelenterate. Science 172,
965 495–498.
966 Nascimento, S.M., Corrêa, E.V., Menezes, M., Varela, D., Paredes, J., Morris, S., 2012. Growth and
967 toxin profile of *Ostreopsis* cf. *ovata* (Dinophyta) from Rio de Janeiro, Brazil. Harmful Algae
968 13, 1–9. https://doi.org/10.1016/j.hal.2011.09.008
969 Neves, R.A.F., Contins, M., Nascimento, S.M., 2018. Effects of the toxic benthic dinoflagellate
970 *Ostreopsis* cf. *ovata* on fertilization and early development of the sea urchin *Lytechinus*
971 *variegatus*. Mar. Environ. Res. 135, 11–17. https://doi.org/10.1016/j.marenvres.2018.01.014
972 Nézan, E., Siano, R., Boulben, S., Six, C., Bilien, G., Chèze, K., Duval, A., Le Panse, S., Quéré, J.,
973 Chomérat, N., 2014. Genetic diversity of the harmful family Kareniaceae (Gymnodiniales,
974 Dinophyceae) in France, with the description of *Karlodinium gentienii* sp. nov.: A new
975 potentially toxic dinoflagellate. Harmful Algae 40, 75–91.
976 https://doi.org/10.1016/j.hal.2014.10.006
977 Norris, D.R., Bomber, J.W., Balech, E., 1985. Benthic dinoflagellates associated with ciguatera
978 from the Florida Keys. I. *Ostreopsis heptagona* sp. nov., in: Anderson, D.M., White, A.W.,
979 Baden, D.G. (Eds.), Toxic Dinoflagellates. Elsevier Science publ. Co., New York, pp. 39–44.
980 Onuma, Y., Satake, M., Ukena, T., Roux, J., Chanteau, S., Rasolofonirina, N., Ratsimaloto, M.,
981 Naoki, H., Yasumoto, T., 1999. Identification of putative palytoxin as the cause of
982 clupeotoxism. Toxicon 37, 55–65.

983 Parsons, M.L., Aligizaki, K., Dechraoui Bottein, M.-Y., Fraga, S., Morton, S.L., Penna, A., Rhodes,
984 L., 2012. *Gambierdiscus* and *Ostreopsis*: Reassessment of the state of knowledge of their
985 taxonomy, geography, ecophysiology, and toxicology. Harmful Algae 14, 107–129.
986 Pavaux, A.-S., Rostan, J., Guidi-Guilvard, L., Marro, S., Ternon, E., Thomas, O.P., Lemée, R.,
987 Gasparini, S., 2019. Effects of the toxic dinoflagellate *Ostreopsis* cf. *ovata* on survival,
988 feeding and reproduction of a phytal harpacticoid copepod. J. Exp. Mar. Biol. Ecol. 516,
989 103–113. https://doi.org/10.1016/j.jembe.2019.05.004
990 Pawlowiez, R., Darius, H.T., Cruchet, P., Rossi, F., Caillaud, A., Laurent, D., Chinain, M., 2013.
991 Evaluation of seafood toxicity in the Australes archipelago (French Polynesia) using the
992 neuroblastoma cell-based assay. Food Addit. Contam. Part A 30, 567–586.
993 https://doi.org/10.1080/19440049.2012.755644
994 Peel, M.C., Finlayson, B.L., McMahon, T.A., 2007. Updated world map of the Ko¨ppen-Geiger
995 climate classification. Hydrol Earth Syst Sci 12.
996 Pelin, M., Forino, M., Brovedani, V., Tartaglione, L., Dell'Aversano, C., Pistocchi, R., Poli, M.,
997 Sosa, S., Florio, C., Ciminiello, P., Tubaro, A., 2016. Ovatoxin-a, A Palytoxin Analogue
998 Isolated from *Ostreopsis* cf. *ovata* Fukuyo: Cytotoxic Activity and ELISA Detection.
999 Environ. Sci. Technol. 50, 1544–1551. https://doi.org/10.1021/acs.est.5b04749
1000 Penna, A., Vila, M., Fraga, S., Giacobbe, M.G., Andreoni, F., Riobó, P., Vernesi, C., 2005.
1001 Characterization of *Ostreopsis* and *Coolia* (Dinophyceae) isolates in the western
1002 mediterranean sea based on morphology, toxicity and internal transcribed spacer 5.8S rDNA
1003 sequences. J. Phycol. 41, 212–225.
1004 Quod, J.-P., 1994. *Ostreopsis mascarenensis* sp. nov. (Dinophyceae), dinoflagellé toxique associé à
1005 la ciguatera dans l'océan Indien. Cryptogam. Algol. 15, 243–251.
1006 Randall, J.E., 2005. Review of clupeotoxism, an often fatal illness from the consumption of
1007 clupeoid fishes. Pac. Sci. 59, 73–77. https://doi.org/10.1353/psc.2005.0013

1008 Rasband, W.S., 1997. ImageJ. National Institutes of Health, Bethesda, Maryland.
1009 Rhodes, L., Adamson, J., Suzuki, T., Briggs, L., Garthwaite, I., 2000. Toxic marine epiphytic
1010 dinoflagellates, *Ostreopsis siamensis* and *Coolia monotis* (Dinophyceae), in New Zealand.
1011 N. Z. J. Mar. Freshw. Res. 34, 371–383.
1012 Rhodes, L., 2011. World-wide occurrence of the toxic dinoflagellate genus *Ostreopsis* Schmidt.
1013 Toxicon 57, 400–407. https://doi.org/10.1016/j.toxicon.2010.05.010
1014 Rhodes, L.L., Smith, K.F., Verma, A., Murray, S., Harwood, D.T., Trnski, T., 2017. The
1015 dinoflagellate genera *Gambierdiscus* and *Ostreopsis* from subtropical Raoul Island and
1016 North Meyer Island, Kermadec Islands. N. Z. J. Mar. Freshw. Res. 51, 490–504.
1017 https://doi.org/10.1080/00288330.2016.1270337
1018 Ronquist, F., Huelsenbeck, J.P., 2003. MrBayes 3: Bayesian phylogenetic inference under mixed
1019 models. Bioinformatics 19, 1572–1574.
1020 Sato, S., Nishimura, T., Uehara, K., Sakanari, H., Tawong, W., Hariganeya, N., Smith, K., Rhodes,
1021 L., Yasumoto, T., Taira, Y., Suda, S., Yamaguchi, H., Adachi, M., 2011. Phylogeography of
1022 *Ostreopsis* along west Pacific coast, with special reference to a novel clade from Japan. Plos
1023 One 6, e27983. https://doi.org/10.1371/journal.pone.0027983
1024 Schiller, J., 1937. Dinoflagellatae (Peridineae), in: Rabenhorst, L. (Ed.), Kryptogamen-Flora von
1025 Deutschland, Österreich Und Der Schweiz, Teil. 2. Academische Verlagsgesellschaft
1026 M.B.H., Leipzig, 589 pp.
1027 Schmidt, J., 1901. Preliminary report of the botanical results of the Danish expedition to Siam
1028 (1899-1900). Part IV, Peridiniales. Bot. Tidsskr. 24, 212–221.
1029 Selina, M.S., Orlova, T.Y., 2010. First occurrence of the genus *Ostreopsis* (Dinophyceae) in the Sea
1030 of Japan. Bot. Mar. 53, 243–249. https://doi.org/10.1515/bot.2010.033

1031 Shears, N.T., Ross, P.M., 2009. Blooms of benthic dinoflagellates of the genus *Ostreopsis*; an
1032 increasing and ecologically important phenomenon on temperate reefs in New Zealand and
1033 worldwide. Harmful Algae 8, 916–925. https://doi.org/10.1016/j.hal.2009.05.003
1034 Smith, K.F., Kohli, G.S., Murray, S.A., Rhodes, L.L., 2017. Assessment of the metabarcoding
1035 approach for community analysis of benthic-epiphytic dinoflagellates using mock
1036 communities. N. Z. J. Mar. Freshw. Res. 51, 555–576.
1037 https://doi.org/10.1080/00288330.2017.1298632
1038 Suzuki, T., Watanabe, R., Uchida, H., Matsushima, R., Nagai, H., Yasumoto, T., Yoshimatsu, T.,
1039 Sato, S., Adachi, M., 2012. LC-MS/MS analysis of novel ovatoxin isomers in several
1040 *Ostreopsis* strains collected in Japan. Harmful Algae 20, 81–91.
1041 https://doi.org/10.1016/j.hal.2012.08.002
1042 Tartaglione, L., Dello Iacovo, E., Mazzeo, A., Casabianca, S., Ciminiello, P., Penna, A.,
1043 Dell'Aversano, C., 2017. Variability in toxin profiles of the Mediterranean *Ostreopsis* cf.
1044 *ovata* and in structural features of the produced ovatoxins. Environ. Sci. Technol. 51,
1045 13920–13928. https://doi.org/10.1021/acs.est.7b03827
1046 Tawong, W., Nishimura, T., Sakanari, H., Sato, S., Yamaguchi, H., Adachi, M., 2014. Distribution
1047 and molecular phylogeny of the dinoflagellate genus *Ostreopsis* in Thailand. Harmful Algae
1048 37, 160–171. https://doi.org/10.1016/j.hal.2014.06.003
1049 Terajima, T., Uchida, H., Abe, N., Yasumoto, T., 2018a. Structure elucidation of ostreocin-A and
1050 ostreocin-E1, novel palytoxin analogs produced by the dinoflagellate *Ostreopsis siamensis* ,
1051 using LC/Q-TOF MS. Biosci. Biotechnol. Biochem. 83, 1–10.
1052 https://doi.org/10.1080/09168451.2018.1550356
1053 Terajima, T., Uchida, H., Abe, N., Yasumoto, T., 2018b. Simple structural elucidation of ostreocin-
1054 B, a new palytoxin congener isolated from the marine dinoflagellate *Ostreopsis siamensis* ,
1055 using complementary positive and negative ion liquid chromatography/quadrupole time-of-

1056 flight mass spectrometry. Rapid Commun. Mass Spectrom. 32, 1001–1007.
1057 https://doi.org/10.1002/rcm.8130
1058 Tester, P.A., Litaker, R.W., Berdalet, E., 2020. Climate change and harmful benthic microalgae.
1059 Harmful Algae 101655. https://doi.org/10.1016/j.hal.2019.101655
1060 Tibiriçá, C.E.J.A., Leite, I.P., Batista, T.V.V., Fernandes, L.F., Chomérat, N., Herve, F., Hess, P.,
1061 Mafra, L.L., 2019. *Ostreopsis* cf. *ovata* bloom in Currais, Brazil: Phylogeny, toxin profile
1062 and contamination of mussels and marine plastic litter. Toxins 11, 446.
1063 https://doi.org/10.3390/toxins11080446
1064 Tichadou, L., Glaizal, M., Armengaud, A., Grossel, H., Lemée, R., Kantin, R., Lasalle, J.-L.,
1065 Drouet, G., Rambaud, L., Malfait, P., de Haro, L., 2010. Health impact of unicellular algae
1066 of the *Ostreopsis* genus blooms in the Mediterranean Sea: experience of the French
1067 Mediterranean coast surveillance network from 2006 to 2009. Clin. Toxicol. 48, 839–844.
1068 https://doi.org/10.3109/15563650.2010.513687
1069 Tognetto, L., Bellato, S., Moro, I., Andreoli, C., 1995. Occurrence of *Ostreopsis ovata*
1070 (Dinophyceae) in the Tyrrhenian Sea during Summer 1994. Bot. Mar. 38.
1071 https://doi.org/10.1515/botm.1995.38.1-6.291
1072 Ukena, T., Satake, M., Usami, M., Oshima, Y., Naoki, H., Fujita, T., Kan, Y., Yasumoto, T., 2001.
1073 Structure elucidation of Ostreocin D, a palytoxin analog isolated from the dinoflagellate
1074 *Ostreopsis siamensis*. Biosci. Biotechnol. Biochem. 65, 2585–2588.
1075 https://doi.org/10.1271/bbb.65.2585
1076 Ukena, T., Satake, M., Usami, M., Oshima, Y., Fujita, T., Naoki, H., Yasumoto, T., 2002. Structural
1077 confirmation of ostreocin-D by application of negative-ion fast-atom bombardment
1078 collision-induced dissociation tandem mass spectrometric methods. Rapid Commun. Mass
1079 Spectrom. 16, 2387–2393. https://doi.org/10.1002/rcm.867

1080 Usami, M., Satake, M., Ishida, S., Inoue, A., Kan, Y., Yasumoto, T., 1995. Palytoxin analogs from
1081 the dinoflagellate *Ostreopsis siamensis*. J. Am. Chem. Soc. 117, 5389–5390.
1082 Verma, A., Hoppenrath, M., Dorantes-Aranda, J.J., Harwood, D.T., Murray, S.A., 2016a. Molecular
1083 and phylogenetic characterization of *Ostreopsis* (Dinophyceae) and the description of a new
1084 species, *Ostreopsis rhodesae* sp. nov., from a subtropical Australian lagoon. Harmful Algae
1085 60, 116–130. https://doi.org/10.1016/j.hal.2016.11.004
1086 Verma, A., Hoppenrath, M., Harwood, T., Brett, S., Rhodes, L., Murray, S., 2016b. Molecular
1087 phylogeny, morphology and toxigenicity of *Ostreopsis* cf. *siamensis* (Dinophyceae) from
1088 temperate south-east Australia. Phycol. Res. 64, 146–159. https://doi.org/10.1111/pre.12128
1089 Vila, M., Garcés, E., Masó, M., 2001. Potentially toxic epiphytic dinoflagellate assemblages on
1090 macroalgae in the NW Mediterranean Marine Science. Aquat. Microb. Ecol. 26, 51–60.
1091 Zhang, H., Lu, S., Li, Y., Cen, J., Wang, H., Li, Q., Nie, X., 2018. Morphology and molecular
1092 phylogeny of *Ostreopsis* cf. *ovata* and *O. lenticularis* (Dinophyceae) from Hainan Island,
1093 South China Sea: *Ostreopsis* spp. from Hainan Island. Phycol. Res. 66, 3–14.
1094 https://doi.org/10.1111/pre.12192
1095

Figure legends

Fig. 1. Map of French Polynesia (South Pacific Ocean) and Tahiti island, showing the location of the Toaroto beach (Punaauia) where the *Ostreopsis* bloom was observed and sampled.

Fig. 2. Photographs of the benthic bloom at Toaroto beach showing the filamentous and mucilaginous brownish biofilm covering abiotic and biotic substrates including (A) macroalgae (*Turbinaria ornata* and *Dictyota bartayresiana*, (B) sponges and (C) corals (*Porites*, *Pocillopora*). (D) Light micrograph of a sample of the bloom dominated by *Ostreopsis* cells and diatoms. Scale bar: 50 µm.

Fig. 3. Light and epifluorescence micrographs of cells from strain PNA19-9 from Toaroto beach (Punaauia, Tahiti island). (A–C) Live specimens: (A) specimen with an oval shape; (B) rounded specimen; (C) lateral view with focus on the undulated cingulum. (D–I) Epifluorescence micrographs: (D) apical view; (E) antapical view; (F) detail of the surface of 2′′′′ plate (G) lateral view showing the undulation of the cingulum; (H) Right ventral view; (I) detail of the apical pore complex (APC) and 2′ plate. Scale bars: 10 µm in A–H, 5 µm in I.

Fig. 4. Scanning electron micrographs of field specimens from the bloom of Toaroto beach (Tahiti island). (A) Apical view; (B) antapical view; (C) apical view of a smaller and less pointed specimen; (D) antapical view of a small and round specimen; (E) ventral view, note the undulated cingulum; (F) ventro-apical view; (G) ventro-antapical view; (H) left lateral view showing the undulated cingulum and apical pore complex; (I) right lateral view. Scale bars: 10 µm.

Fig. 5. Scanning electron micrographs of field specimens from the bloom of Toaroto beach (Tahiti island). (A) Detail of apical plate series and apical pore; (B) detail of the second apical (2′) plate and Po plate; (C) detail of the ventral area, with the ventral opening (Vo) and list of the Sda plate (black arrowhead) visible; (D) antapical view of the sulcal area; (E) ventral view of the sulcus; (F) detail of the sulcal plates; (G) sulcal plates on a broken specimen, note the ventral opening within the Ssa plate; (H-I) Thecal pores of two sizes, note that the internal structure is visible within larger pores; (J) internal view of thecal plates, with smaller thecal pores better visible. Scale bars: 2 µm in A, B, C, D, E and G, 1 µm in F, and 500 nm in H, I and J.

Fig. 6. Maximum Likelihood phylogenetic tree inferred from LSU rDNA D8–D10 sequences of various *Ostreopsis* strains and field specimens. Sequences from the present study are in bold face on a gray background. *Coolia* sp. is used as an outgroup. Black vertical bars show distinct *Ostreopsis* clades. Numbers at nodes represent bootstrap support values from Maximum Likelihood (ML) and posterior probabilities from Bayesian Inference (BI). Bootstraps values below 65 and posterior probabilities below 0.70 are indicated with '-'.

Fig. 7. Maximum Likelihood phylogenetic tree inferred from LSU rDNA D1–D3 sequences of various *Ostreopsis* strains and field specimens. Sequences from the present study are in bold face on a gray background. *Coolia monotis* is used as an outgroup. Black vertical bars show distinct *Ostreopsis* clades. Numbers at nodes represent bootstrap support values from Maximum Likelihood (ML) and posterior probabilities from Bayesian Inference (BI). Bootstraps values below 65 and posterior probabilities below 0.70 are indicated with '-'.

1142 **Fig. 8.** Maximum Likelihood phylogenetic tree inferred from ITS–5.8S rDNA sequences of various
1143 *Ostreopsis* strains and field specimens. *Ostreopsis mascarenensis and Ostreopsis* sp. 4 are used as
1144 outgroup. Sequence from the present study are by bold face on a gray background. Black vertical
1145 bars show distinct *Ostreopsis* clade. Numbers at nodes represent bootstrap support values from
1146 Maximum Likelihood (ML) and posterior probabilities from Bayesian Inference (BI). Bootstraps
1147 values below 65 are indicated with '-'.

1148

1149 **Fig. 9.** Toxicity of *Ostreopsis* sp. 6 (strain PNA19-1) as assessed by means of the CBA-N2a. Dose-
1150 response curves of Neuro-2a cells when exposed to increasing concentrations of (A) standard of
1151 PlTX and (B) cell extract of strain PNA19-1. Data represent the mean $\pm$ SD of each concentration
1152 run in triplicate in three independent experiments (n = 3), in the absence (O^- condition, dotted lines)
1153 vs. presence of 200 µM Ouabain (O^+ conditions, plain lines). The EC_{50} values obtained in O^- and O^+
1154 conditions were estimated at 1,074 ± 23 and 156 ± 17 pg. mL^{-1} for PlTX, and 564 ± 19 and 137 ±
1155 13 cell equiv. mL^{-1} for strain PNA19-1.

1156

1157 **Fig. 10.** Toxin contents and profiles of the eight *Ostreopsis* strains isolated from the Toaroto bloom
1158 analyzed by LC-MS/MS.

1159

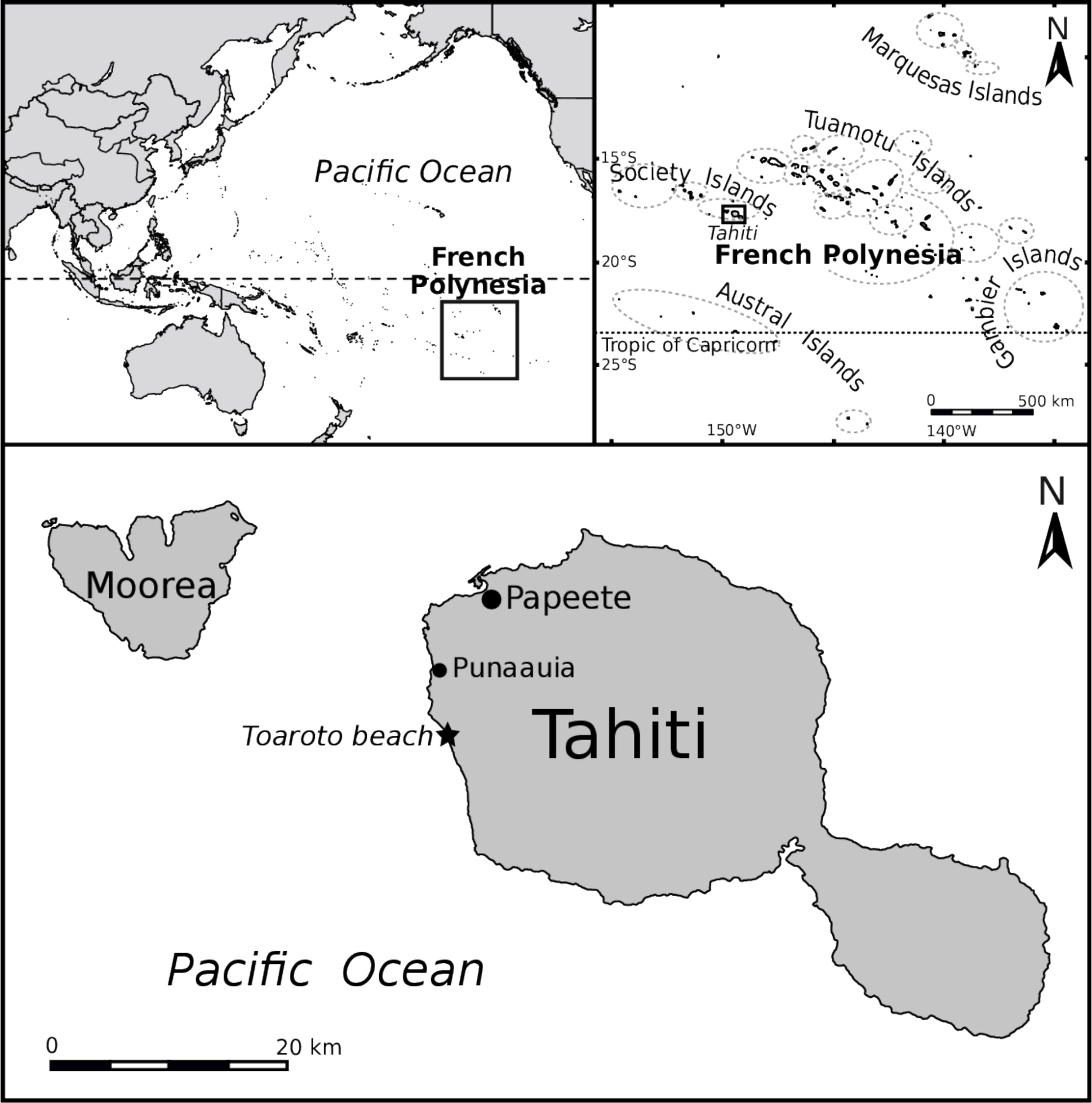
Pacific Ocean
French Polynesia
N
Marquesas Islands
Tuamotu Islands
Society Islands
Tahiti
French Polynesia
Gambier Islands
Austral Islands
Tropic of Capricorn
15°S
20°S
25°S
150°W
140°W
0
500 km
Moorea
Papeete
Punaauia
Tahiti
Toaroto beach
Pacific Ocean
0
20 km


A
B
C
D

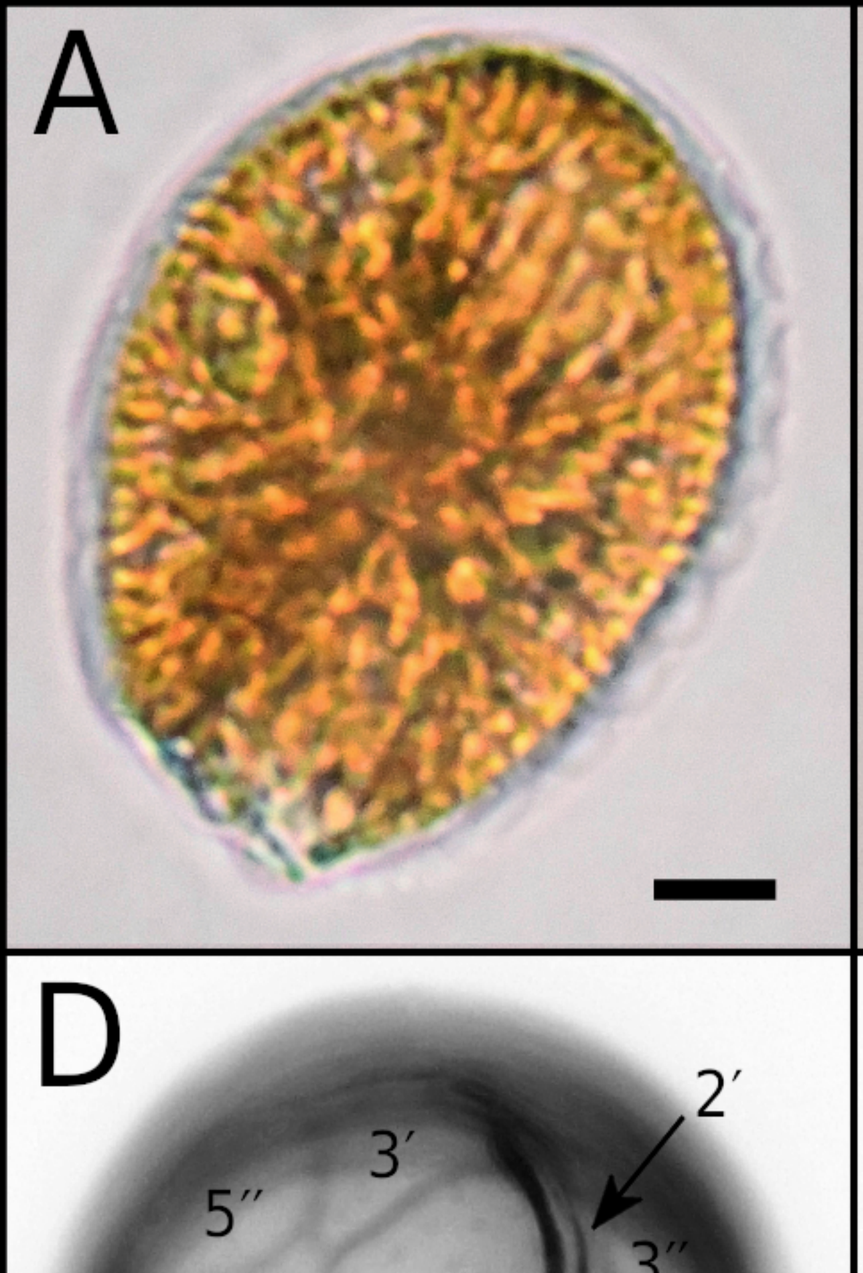
A


B

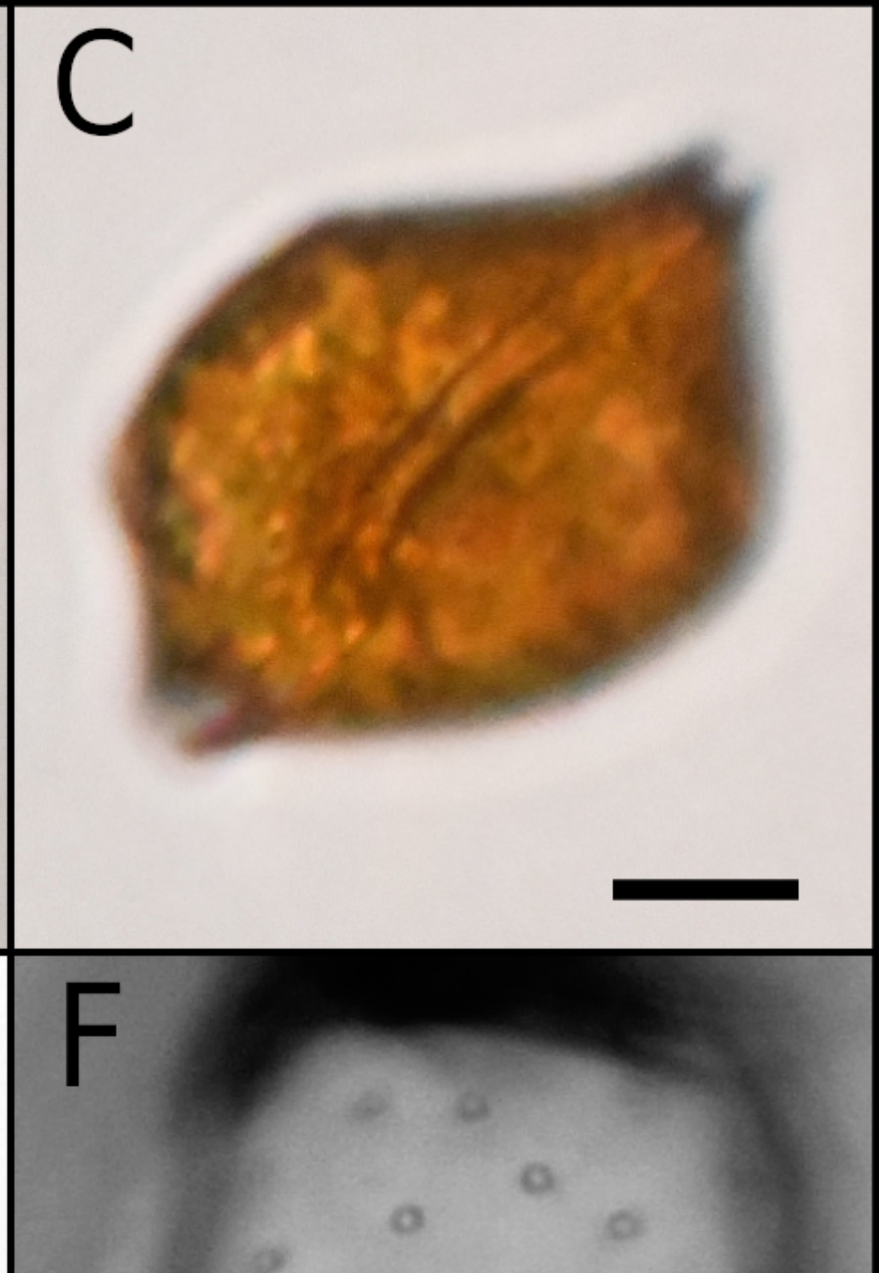
C

D
2′
3′
5″
3″
6″
1′
2″
7″
1″

E
1‴′
5‴
2‴′
2‴
4‴
3‴

F
2‴′

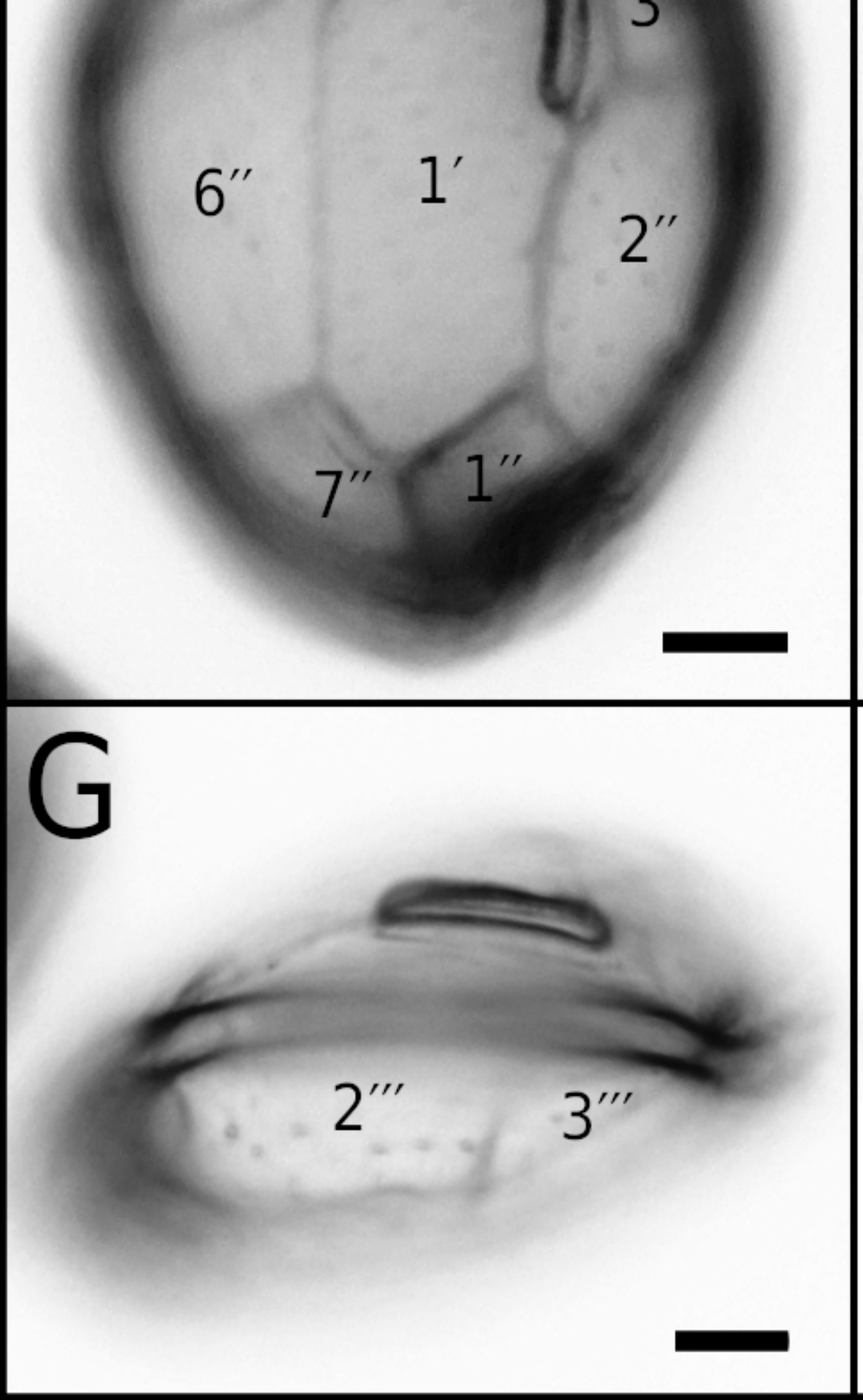
G
2‴
3‴

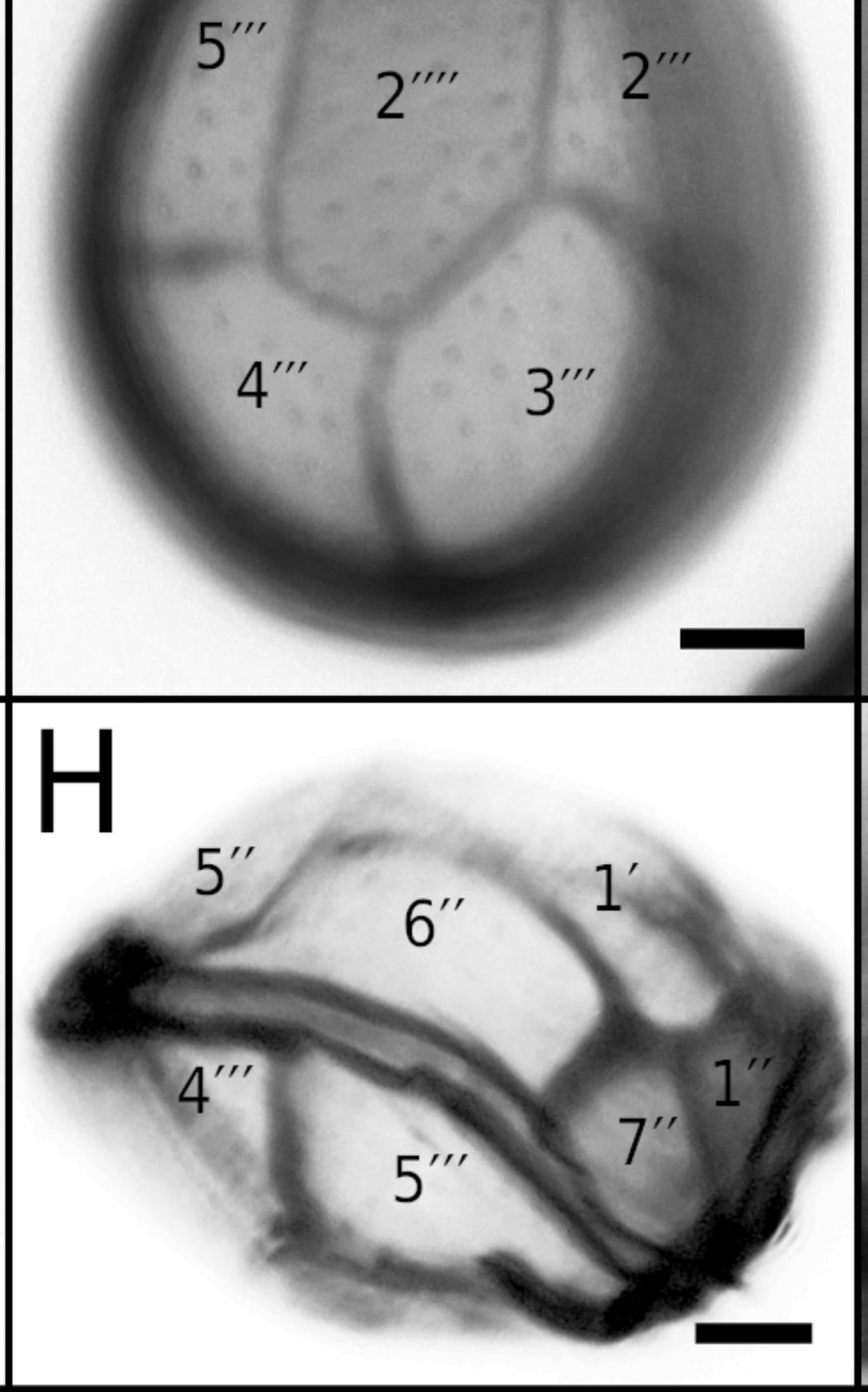
H
5″
6″
1′
4‴
1″
7″
5‴

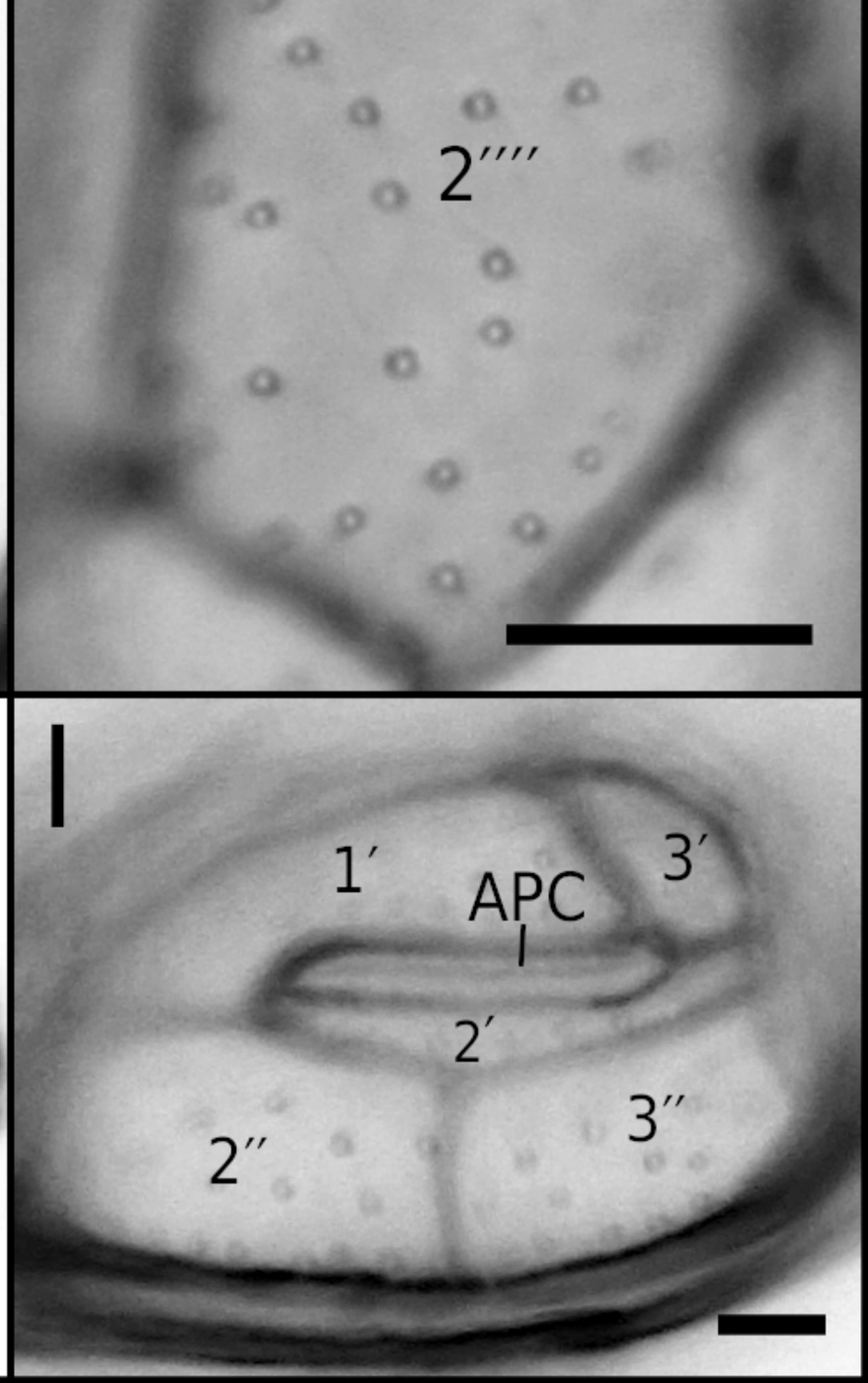
I
1′
APC
3′
2′
2″
3″

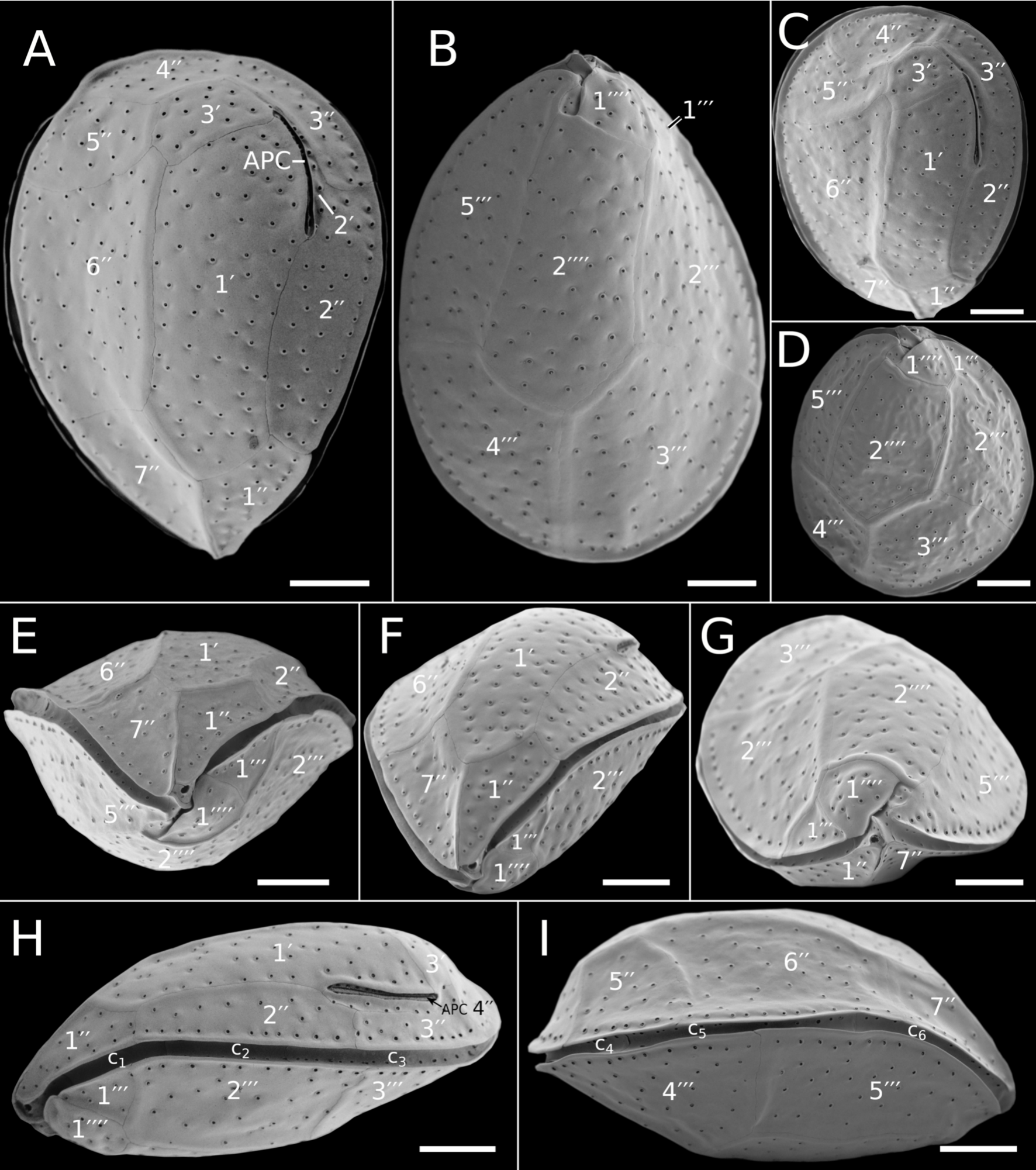
A
4″
3′
3″
5″
APC
2′
6″
1′
2″
7″
1″
B
1‴′
1‴
5‴
2‴′
2‴
4‴
3‴
C
4″
3′
3″
5″
1′
6″
2″
7″
1″
D
1‴′
1‴
5‴
2‴′
2‴
4‴
3‴
E
1′
6″
2″
7″
1″
1‴
2‴
5‴
1‴′
2‴′
F
1′
6″
2″
7″
1″
2‴
1‴
1‴′
G
3‴
2‴′
2‴
1‴′
5‴
1‴
1″
7″
H
1′
3
2″
APC 4″
3″
1″
c1
c2
c3
1‴
2‴
3‴
1‴′
I
6″
5″
7″
c4
c5
c6
4‴
5‴

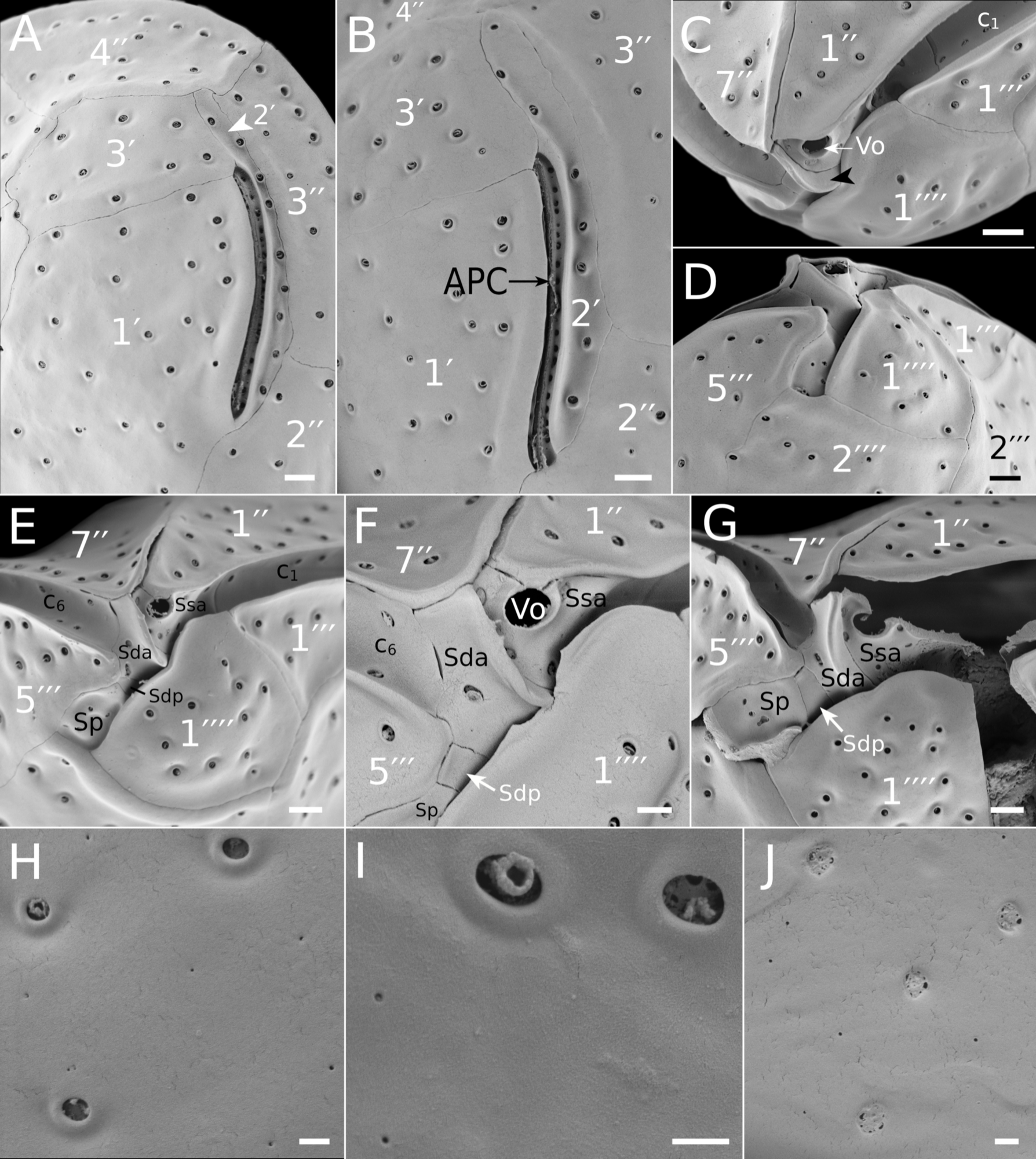
A
4‴
2′
3′
3‴
1′
2″
B
4″
3‴
3′
APC
2′
1′
2″
C
c1
1″
7″
1‴
Vo
1⁗
D
1‴
1⁗
5‴
2⁗
2‴
E
1″
7″
c1
c6
Ssa
1‴
Sda
5‴
Sdp
Sp
1⁗
F
1″
7″
Vo
Ssa
c6
Sda
5‴
Sdp
Sp
1⁗
G
1″
7″
5⁗
Ssa
Sda
Sp
Sdp
1⁗
H
I
J

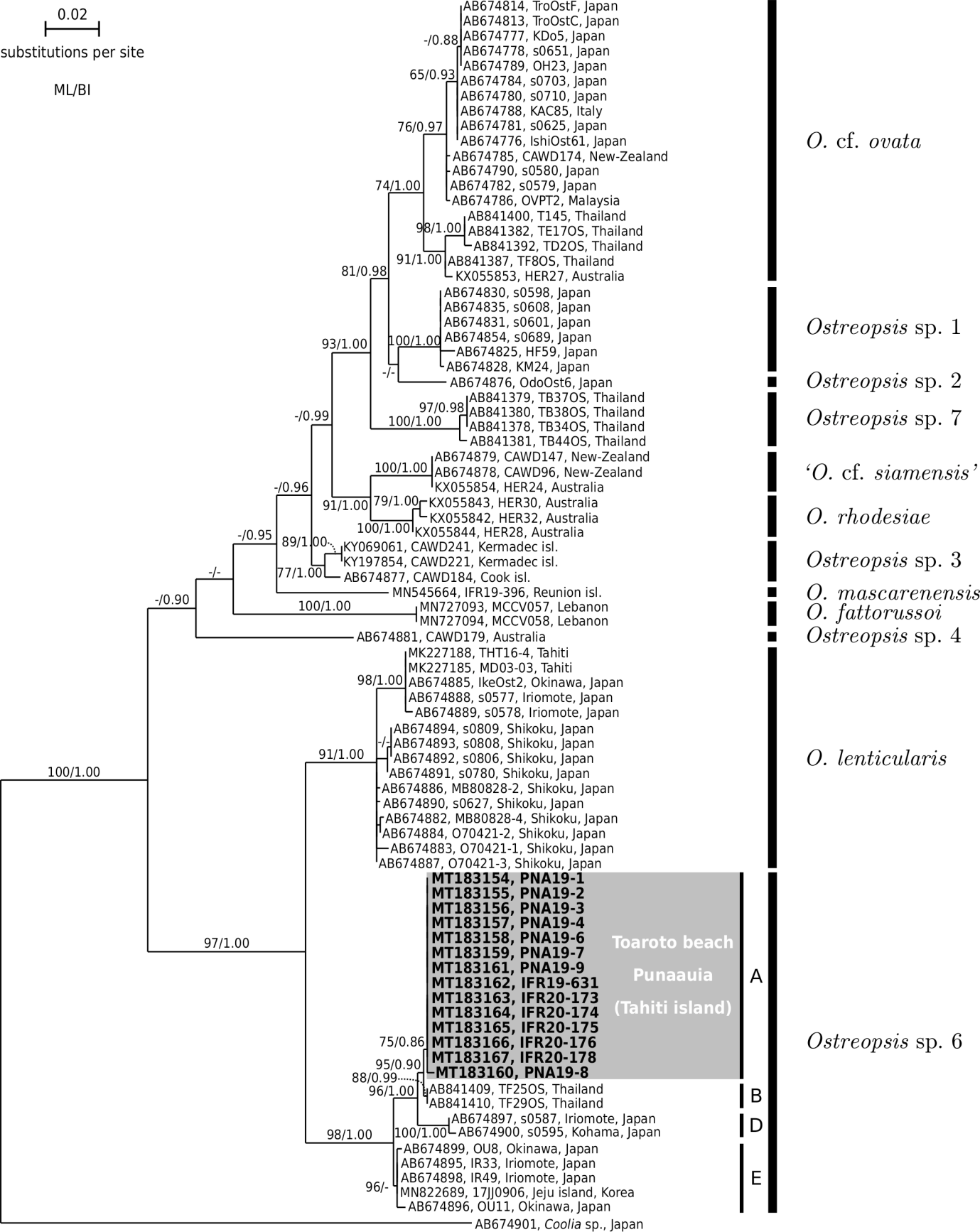
0.02
substitutions per site
ML/BI
AB674814, TroOstF, Japan
AB674813, TroOstC, Japan
-/0.88
AB674777, KDo5, Japan
AB674778, s0651, Japan
AB674789, OH23, Japan
65/0.93
AB674784, s0703, Japan
AB674780, s0710, Japan
AB674788, KAC85, Italy
AB674781, s0625, Japan
76/0.97
AB674776, IshiOst61, Japan
AB674785, CAWD174, New-Zealand
AB674790, s0580, Japan
74/1.00
AB674782, s0579, Japan
AB674786, OVPT2, Malaysia
AB841400, T145, Thailand
98/1.00
AB841382, TE17OS, Thailand
AB841392, TD2OS, Thailand
91/1.00
AB841387, TF8OS, Thailand
81/0.98
KX055853, HER27, Australia
O. cf. ovata
AB674830, s0598, Japan
AB674835, s0608, Japan
AB674831, s0601, Japan
93/1.00
100/1.00
AB674854, s0689, Japan
AB674825, HF59, Japan
AB674828, KM24, Japan
-/-
AB674876, OdoOst6, Japan
Ostreopsis sp. 1
Ostreopsis sp. 2
AB841379, TB37OS, Thailand
97/0.98
AB841380, TB38OS, Thailand
-/0.99
100/1.00
AB841378, TB34OS, Thailand
AB841381, TB44OS, Thailand
Ostreopsis sp. 7
AB674879, CAWD147, New-Zealand
100/1.00
AB674878, CAWD96, New-Zealand
KX055854, HER24, Australia
'O. cf. siamensis'
-/0.96
79/1.00
KX055843, HER30, Australia
91/1.00
KX055842, HER32, Australia
100/1.00
KX055844, HER28, Australia
O. rhodesiae
-/0.95
89/1.00
KY069061, CAWD241, Kermadec isl.
KY197854, CAWD221, Kermadec isl.
-/-
77/1.00
AB674877, CAWD184, Cook isl.
Ostreopsis sp. 3
MN545664, IFR19-396, Reunion isl.
O. mascarenensis
-/0.90
100/1.00
MN727093, MCCV057, Lebanon
MN727094, MCCV058, Lebanon
O. fattorussoi
AB674881, CAWD179, Australia
Ostreopsis sp. 4
MK227188, THT16-4, Tahiti
MK227185, MD03-03, Tahiti
98/1.00
AB674885, IkeOst2, Okinawa, Japan
AB674888, s0577, Iriomote, Japan
AB674889, s0578, Iriomote, Japan
AB674894, s0809, Shikoku, Japan
-/-
AB674893, s0808, Shikoku, Japan
91/1.00
AB674892, s0806, Shikoku, Japan
AB674891, s0780, Shikoku, Japan
100/1.00
AB674886, MB80828-2, Shikoku, Japan
AB674890, s0627, Shikoku, Japan
AB674882, MB80828-4, Shikoku, Japan
AB674884, O70421-2, Shikoku, Japan
AB674883, O70421-1, Shikoku, Japan
AB674887, O70421-3, Shikoku, Japan
O. lenticularis
MT183154, PNA19-1
MT183155, PNA19-2
MT183156, PNA19-3
MT183157, PNA19-4
MT183158, PNA19-6
MT183159, PNA19-7
MT183161, PNA19-9
MT183162, IFR19-631
MT183163, IFR20-173
MT183164, IFR20-174
MT183165, IFR20-175
MT183166, IFR20-176
MT183167, IFR20-178
MT183160, PNA19-8
Toaroto beach
Punaauia
(Tahiti island)
A
97/1.00
75/0.86
95/0.90
88/0.99
96/1.00
AB841409, TF25OS, Thailand
AB841410, TF29OS, Thailand
B
AB674897, s0587, Iriomote, Japan
D
98/1.00
100/1.00
AB674900, s0595, Kohama, Japan
AB674899, OU8, Okinawa, Japan
AB674895, IR33, Iriomote, Japan
AB674898, IR49, Iriomote, Japan
96/-
MN822689, 17JJ0906, Jeju island, Korea
AB674896, OU11, Okinawa, Japan
E
Ostreopsis sp. 6
AB674901, Coolia sp., Japan

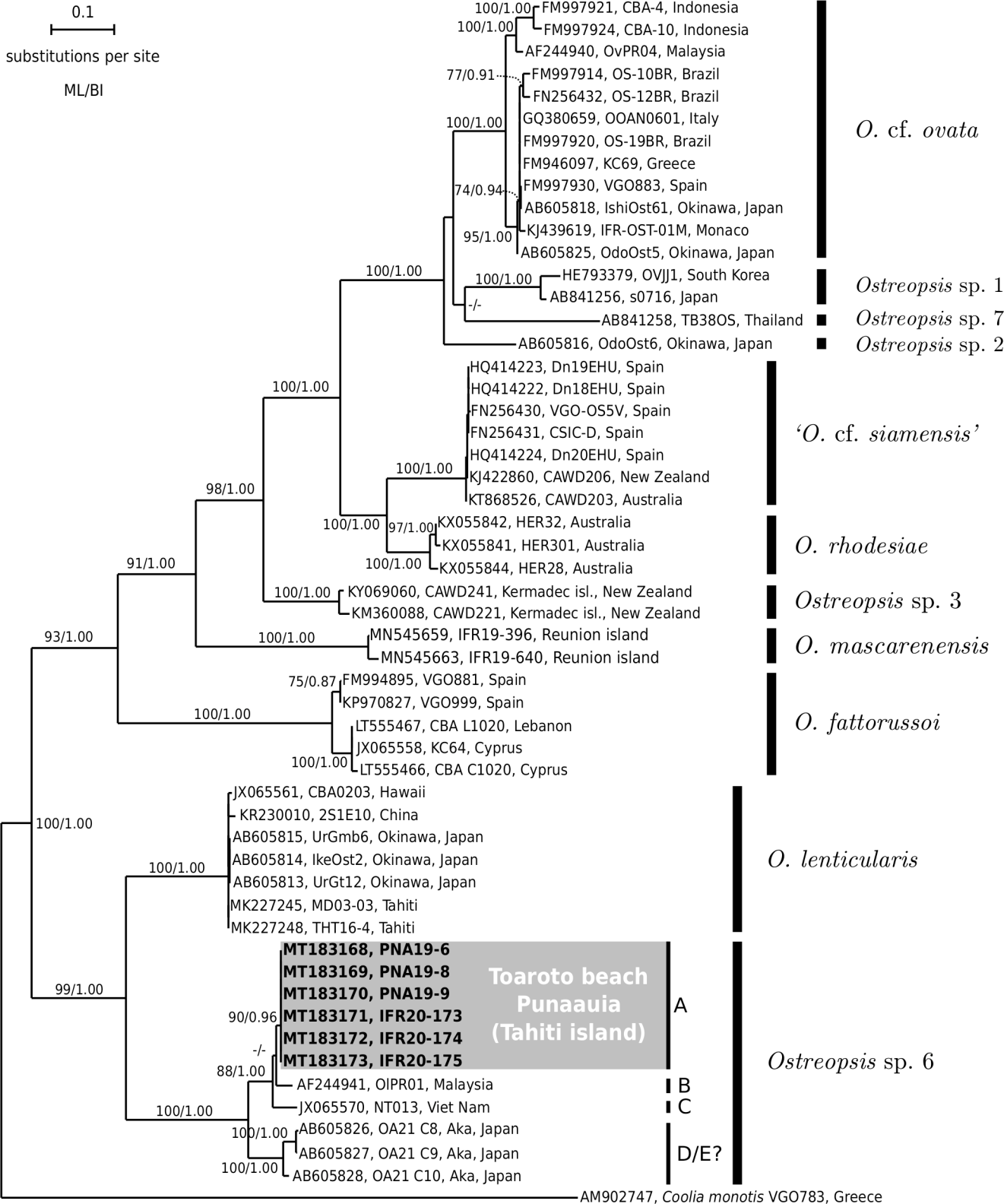
0.1
substitutions per site
ML/BI
100/1.00 FM997921, CBA-4, Indonesia
100/1.00 FM997924, CBA-10, Indonesia
AF244940, OvPR04, Malaysia
77/0.91 FM997914, OS-10BR, Brazil
FN256432, OS-12BR, Brazil
100/1.00 GQ380659, OOAN0601, Italy
FM997920, OS-19BR, Brazil
FM946097, KC69, Greece
74/0.94 FM997930, VGO883, Spain
AB605818, IshiOst61, Okinawa, Japan
95/1.00 KJ439619, IFR-OST-01M, Monaco
AB605825, OdoOst5, Okinawa, Japan
O. cf. ovata
100/1.00
100/1.00 HE793379, OVJJ1, South Korea
AB841256, s0716, Japan
Ostreopsis sp. 1
-/- AB841258, TB38OS, Thailand
Ostreopsis sp. 7
AB605816, OdoOst6, Okinawa, Japan
Ostreopsis sp. 2
100/1.00
HQ414223, Dn19EHU, Spain
HQ414222, Dn18EHU, Spain
FN256430, VGO-OS5V, Spain
FN256431, CSIC-D, Spain
HQ414224, Dn20EHU, Spain
100/1.00 KJ422860, CAWD206, New Zealand
KT868526, CAWD203, Australia
'O. cf. siamensis'
98/1.00
100/1.00
97/1.00 KX055842, HER32, Australia
KX055841, HER301, Australia
100/1.00 KX055844, HER28, Australia
O. rhodesiae
91/1.00
100/1.00 KY069060, CAWD241, Kermadec isl., New Zealand
KM360088, CAWD221, Kermadec isl., New Zealand
Ostreopsis sp. 3
93/1.00
100/1.00 MN545659, IFR19-396, Reunion island
MN545663, IFR19-640, Reunion island
O. mascarenensis
75/0.87 FM994895, VGO881, Spain
KP970827, VGO999, Spain
100/1.00
LT555467, CBA L1020, Lebanon
JX065558, KC64, Cyprus
100/1.00 LT555466, CBA C1020, Cyprus
O. fattorussoi
JX065561, CBA0203, Hawaii
KR230010, 2S1E10, China
AB605815, UrGmb6, Okinawa, Japan
100/1.00
AB605814, IkeOst2, Okinawa, Japan
AB605813, UrGt12, Okinawa, Japan
MK227245, MD03-03, Tahiti
MK227248, THT16-4, Tahiti
O. lenticularis
100/1.00
99/1.00
MT183168, PNA19-6
MT183169, PNA19-8
MT183170, PNA19-9
90/0.96 MT183171, IFR20-173
MT183172, IFR20-174
-/- MT183173, IFR20-175
Toaroto beach
Punaauia
(Tahiti island)
A
88/1.00 AF244941, OlPR01, Malaysia
B
100/1.00 JX065570, NT013, Viet Nam
C
100/1.00 AB605826, OA21 C8, Aka, Japan
AB605827, OA21 C9, Aka, Japan
100/1.00 AB605828, OA21 C10, Aka, Japan
D/E?
Ostreopsis sp. 6
AM902747, Coolia monotis VGO783, Greece

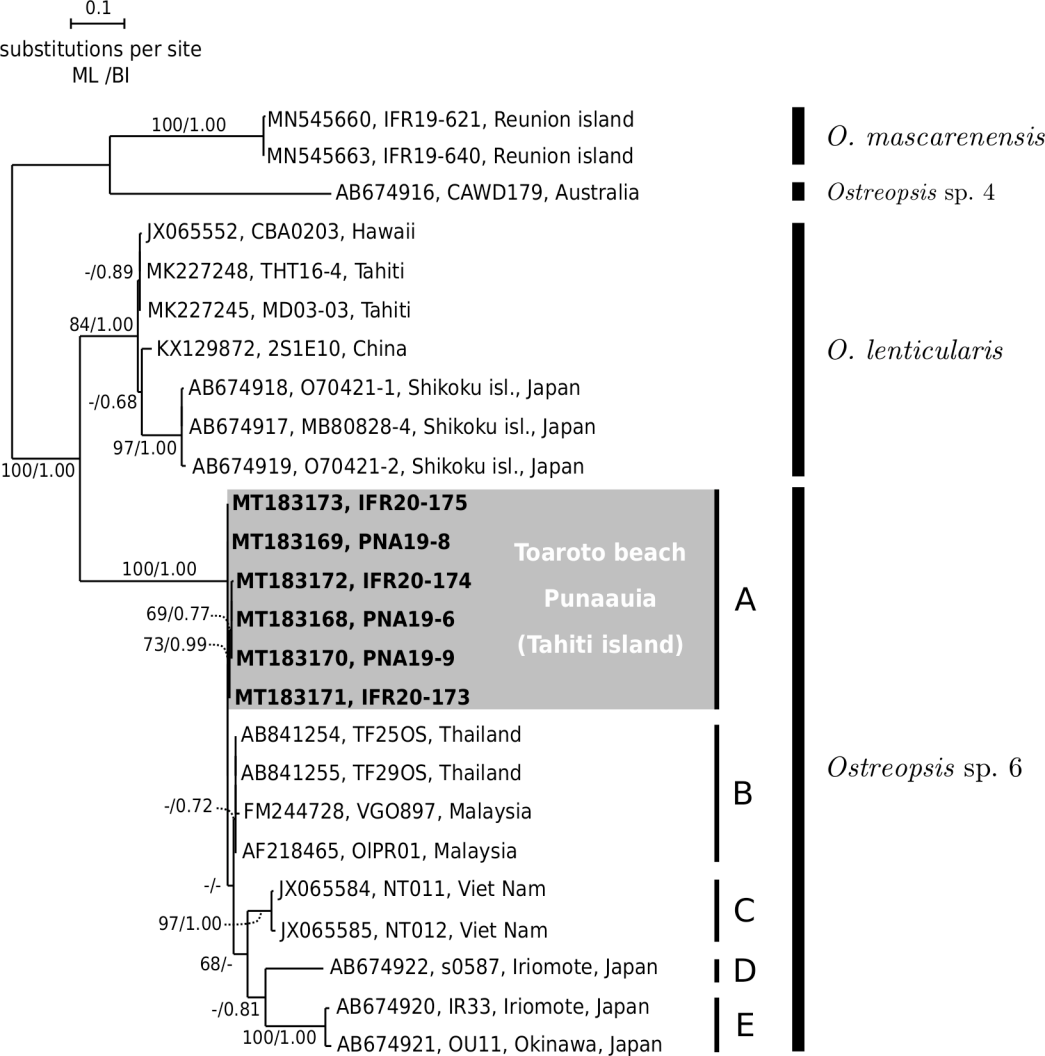
0.1
substitutions per site
ML /BI
100/1.00
MN545660, IFR19-621, Reunion island
MN545663, IFR19-640, Reunion island
AB674916, CAWD179, Australia
O. mascarenensis
Ostreopsis sp. 4
JX065552, CBA0203, Hawaii
-/0.89
MK227248, THT16-4, Tahiti
MK227245, MD03-03, Tahiti
84/1.00
KX129872, 2S1E10, China
-/0.68
AB674918, O70421-1, Shikoku isl., Japan
AB674917, MB80828-4, Shikoku isl., Japan
97/1.00
AB674919, O70421-2, Shikoku isl., Japan
O. lenticularis
100/1.00
MT183173, IFR20-175
MT183169, PNA19-8
Toaroto beach
Punaauia
(Tahiti island)
100/1.00
MT183172, IFR20-174
69/0.77
MT183168, PNA19-6
73/0.99
MT183170, PNA19-9
MT183171, IFR20-173
A
AB841254, TF25OS, Thailand
AB841255, TF29OS, Thailand
-/0.72
FM244728, VGO897, Malaysia
AF218465, OlPR01, Malaysia
B
-/-
JX065584, NT011, Viet Nam
97/1.00
JX065585, NT012, Viet Nam
C
68/-
AB674922, s0587, Iriomote, Japan
D
-/0.81
AB674920, IR33, Iriomote, Japan
100/1.00
AB674921, OU11, Okinawa, Japan
E
Ostreopsis sp. 6

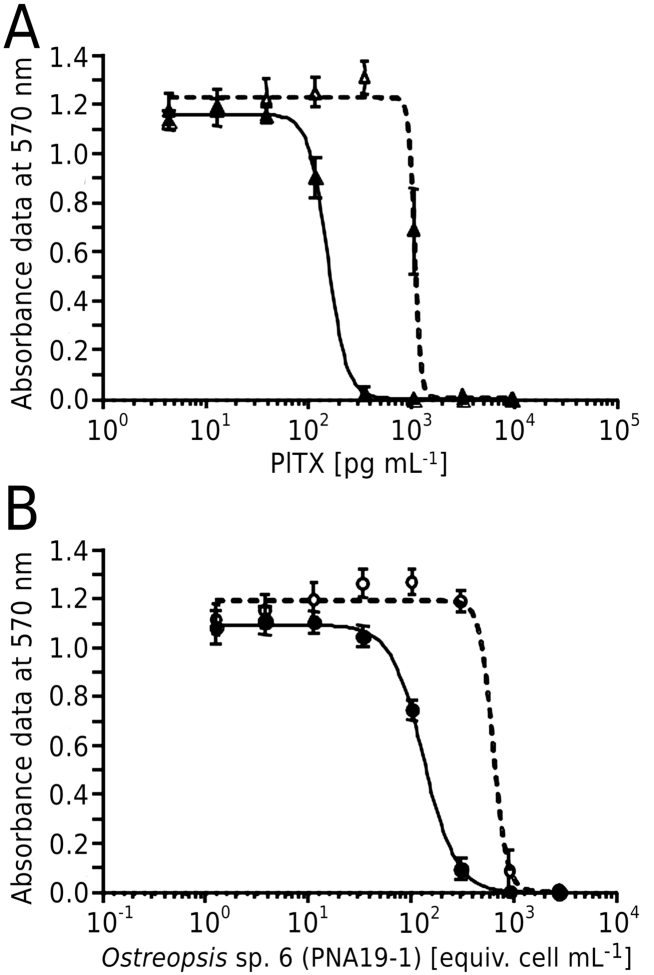
A
Absorbance data at 570 nm
1.4
1.2
1.0
0.8
0.6
0.4
0.2
0.0
10^0
10^1
10^2
10^3
10^4
10^5
PITX [pg mL^{-1}]
B
Absorbance data at 570 nm
1.4
1.2
1.0
0.8
0.6
0.4
0.2
0.0
10^{-1}
10^0
10^1
10^2
10^3
10^4
Ostreopsis sp. 6 (PNA19-1) [equiv. cell mL^{-1}]

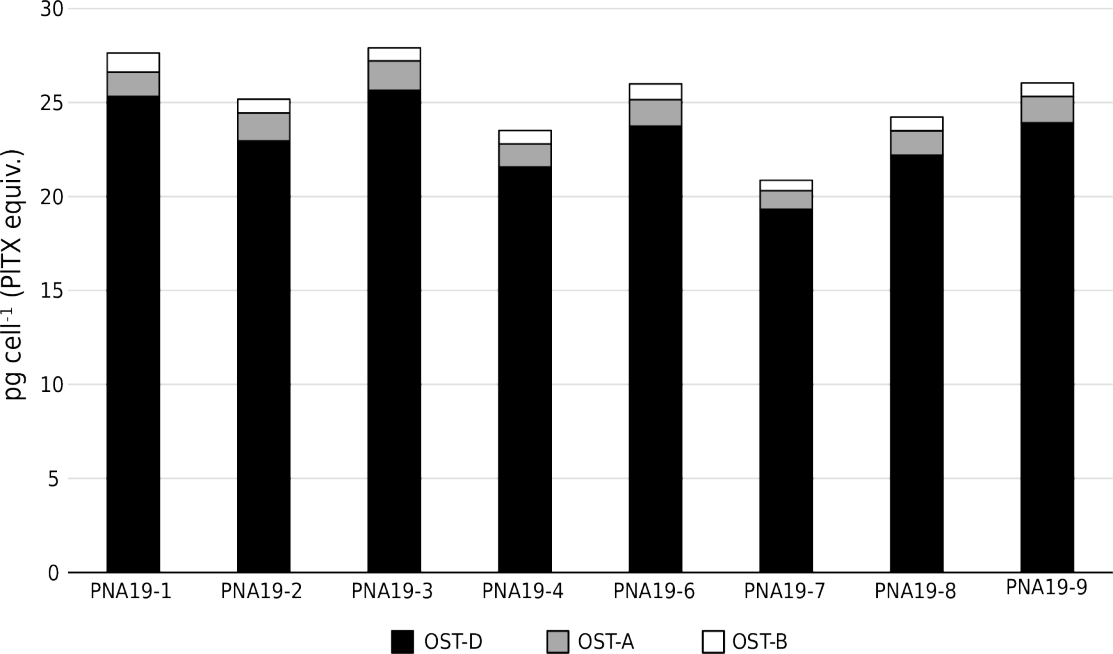
30
25
20
15
10
5
0
pg cell-1 (PlTX equiv.)
PNA19-1
PNA19-2
PNA19-3
PNA19-4
PNA19-6
PNA19-7
PNA19-8
PNA19-9
OST-D
OST-A
OST-B

Table 1. Distance values (pairwise uncorrected *p*-distances) based on the LSU D8–D10 rDNA, LSU D1–D3 rDNA and ITS–5.8S region sequences net-between and within subclades of *Ostreopsis* sp. 6.

LSU rDNA D8 – D10			subclades			
subclades	locality	n	A	B	D	E
A	Tahiti island	14	0.000			
B	Gulf of Thailand	2	0.002	0.000		
D	Iriomote / Kohama islands, Japan	2	0.013	0.013	0.002	
E	Iriomote / Okinawa islands, Japan; Korea	5	0.013	0.012	0.018	0.001

LSU rDNA D1–D3

subclades	locality	n	A	B	C	D/E?
A	Tahiti island	6	0.001			
B	Malaysia	1	0.032	n/c		
C	Viet Nam	1	0.046	0.059	n/c	
D/E?	Aka island, Japan	3	0.094	0.105	0.118	0.023

ITS–5.8S region

subclades	locality	n	A	B	C	D	E
A	Tahiti island	6	0.002				
B	Gulf of Thailand, Malaysia	4	0.008	0.004			
C	Viet Nam	2	0.074	0.068	0.008		
D	Iriomote island (Haemida), Japan	1	0.147	0.141	0.131	n/c	
E	Iriomote (Uehara), Okinawa (Uken) islands, Japan	2	0.127	0.126	0.152	0.150	0.018

Pairwise uncorrected *p* distance values within subclade are shown on the diagonal
n/c: not calculated

Table 2. Estimation of the toxin content of eight strains of *Ostreopsis* sp. 6 in the absence (O^- conditions) and presence (O^+ conditions) of 200 µM ouabain, as assessed by CBA-N2a. For each strain, data represent the mean ± SD of three independent experiments

	O^- condition			O^+ condition		
Strain	pg PlTX equiv. $cell^{-1}$	SD	CV (%)	pg PlTX equiv. $cell^{-1}$	SD	CV (%)
PNA19-1	1.73	0.31	17.8	1.14	0.12	10.6
PNA19-2	2.18	0.09	4.2	1.36	0.08	5.8
PNA19-3	1.99	0.23	11.5	1.17	0.03	2.9
PNA19-4	1.95	0.17	8.7	1.08	0.09	8.0
PNA19-6	2.39	0.11	4.6	1.40	0.14	10.3
PNA19-7	2.48	0.22	8.7	1.31	0.08	6.0
PNA19-8	2.28	0.34	14.9	1.32	0.06	4.2
PNA19-9	2.25	0.11	4.7	1.35	0.07	5.2

Table 3. Morphological data of *O. siamensis*, *O. labens* and *Ostreopsis* sp. 6 from the tropical areas, compared with '*O.* cf. *siamensis*' from the temperate/subtropical areas

Species	Subclade (this study)	DV length (µm)	Width (µm)	DV/W	cingulum	Po plate (µm)	Thecal pores	Ocean/Sea	Study area (latitude)	Köppen-Geiger climate category[1]	Reference
O. siamensis	—	90F	—	—	undulated	—	1 type: large pores (Figs 5-6)	Gulf of Thailand	(≈12°N)	Am (tropical monsoon)	Schmidt (1901)
O. siamensis	—	60–100F	45–90F	—	undulated	—	1 type, large	Pacific Ocean	Ryukyu islands, Japan (≈24–26°N)	Cfa (subtropical humid) to Af (tropical rainforest)	Fukuyo (1981)
O. cf. *siamensis*	—	88–115F	64–93F	0.9–1.6	—	—	1 type: large	Coral Sea	Heron and Lady Elliot islands, Hoffmans	Cwa (subtropical humid)	Holmes et al. (1988)

									rocks Australia (≈24°S)		
'O. lenticularis'† (misidentified)	—	65–75F	57–63F	—	—	16	1 type: large (0.4 µm)	Caribbean Sea region; Indian Ocean ; Pacific Ocean (cf. Fukuyo 1981)	Various islands (≈17°N); Réunion Island (≈21°S);	Am (tropical monsoon, Aw (tropical savanna)	Faust et al. (1996)
O. labens	—	81–110F 86–98F	70–80F	—	undulated (Fig. 6)	18	1 type: large (0.3 µm)	Caribbean Sea Pacific Ocean	Belize (≈17°N) Ishigaki and Iriomote islands, Japan (≈24°N)	Am (tropical monsoon)	Faust and Morton (1995) Faust et al. (1996)

Ostreopsis sp. 6 (as '*O. lenticularis*')	B	64–76C	52–65C	—	—	—	1 type	South China Sea	Pulau Redang (≈6°N)	Aw (tropical savanna)	Leaw et al. (2001)
Ostreopsis sp. 6	B	49.9–84.3C	35.4–66.9C	1.2–1.4	undulated	16	1 type: large (0.35–0.60 µm)	Gulf of Thailand	(≈12°N)	Am (tropical monsoon)	Tawong et al. (2014)
Ostreopsis sp. 6 (strain 17JJ0908)	E	43–69C	36–54	1–1.4	undulated	—	— (large pores visible on pictures)	Yellow Sea	South Korea (Jeju Island, ≈34°N)	Cfa (subtropical humid)	Lee and Park (2020)
Ostreopsis sp. 6	A	58.0–82.5F	45.7–61.2F	1.1–1.5	undulated	17.5	2 types: large (0.34–0.65 µm) and small (0.05–0.08 µm)	Pacific Ocean	French Polynesia, Tahiti island (≈17°S)	Aw (tropical savanna)	**This study**
'*O. siamensis*'†		60–85F	38–45F	—	—	—	2 types: large	Pacific Ocean	Northern	Cfb (warm	Chang et al. (2000)

						(0.18–0.38 µm) and small (0.08 – 0.1 µm)		New Zealand (≈35°S)	temperate oceanic)	
'*O. siamensis*'†	52–68C 30–40C	40–55C 20–30C	—	slight undulation?	11 (from Fig. 2C)	1 type	Pacific Ocean	Northern New Zealand (≈35°S)	Cfb (warm temperate oceanic)	Rhodes et al. (2000)
Ostreopsis sp.	63–90F	34–56F	—	—	10	1 type: 0.1–0.2 µm	Western Mediterranean Sea	Coasts of Spain, Majorca, Corsica (≈41–42°N)	Csa (warm Mediterranean)	Vila et al. (2001)
O. cf. *siamensis*	63–90F 50–75C	34–56F 38–62C	—	flat, not undulated	—	1 type: 0.11–0.56 µm	Mediterranean Sea	Spain, Italy (≈37–44°N)	Csa (warm Mediterranean)	Penna et al. (2005)
O. cf. *siamensis*	36–66F	24–50F	—	straight, sometimes	≈11	1 type: 0.23–0.29 µm	North Aegean Sea	(≈39–41°N)	Csa (warm Mediterranean)	Aligizaki and Nikolaidis (2006)

				undulated						
O. cf. *siamensis*	63–78F	36–54F	1.3–1.9	straight to slightly undulated	10 (from Fig. 17)	1 type: 0.14–0.32 µm	Sea of Japan, Russia	(≈43°N)	Dwb (humid continental)	Selina and Orlova (2010)
O. cf. *siamensis*	51–67C	33–56C	—	—	7–9	1 type: 0.15–0.31 µm	Atlantic Ocean and Mediterranean Sea	Northern Spain (≈43°N) (Minorca, ≈39°N)	Cfb (temperate oceanic) and Csa (warm Mediterranean)	Laza-Martinez et al. (2011)
O. cf. *siamensis*	50–62C	41–50C	1.10–1.32	—	—	1 type	Mediterranean Sea / Atlantic Ocean	(≈37°N)	Csa (warm Mediterranean)	Ciminiello et al. (2013)
O. cf. *siamensis*	52–74.5F	27–57F	1.1–2.1	not undulated	10–12	2 types: large (0.15–0.39 µm) and small (0.07–0.13 µm)	Atlantic Ocean	Coast of Iberian peninsula (≈37–44°N)	Csa (warm Mediterranean) to Cfb (temperate oceanic)	David et al. (2013)

O. cf. *siamensis* (strain HER24)	32.3–46.9C	23.9–37.1	1.2–1.4	—	—	Coral Sea	Heron Island, Australia (≈23°S)	Cwa (subtropical humid)	Verma et al. (2016a)
O. cf. *siamensis*	34–47C	24.5–42C	1.1–1.7	straight	7.2–8.4	2 types	Tasman Sea (South Pacific Ocean)	Merimbula, South-east Australia (≈37°S)	Cfb (warm temperate oceanic)	Verma et al. (2016b)

† our quotation marks, indicating putatively doubtful identifications; —: no data available; F: field specimens, C: cultured cells

[1]from the data of Peel et al. (2007) and Beck et al. (2018)